Science of the Total Environment 1024 (2026) 181643

Contents lists available at ScienceDirect

Science of the Total Environment

journal homepage: www.elsevier.com/locate/scitotenv

Soil organic matter stabilization varies with nitrogen enrichment and hydrogeomorphic setting in a marsh–mangrove ecotone

Mercedes M. Pinzon [a], Jocelyn Bravo [b], Samantha K. Chapman [b], J. Adam Langley [b], Lisa G. Chambers [a,*]

[a] Aquatic Biogeochemistry Laboratory, University of Central Florida, Orlando, FL, USA
[b] Department of Biology, Villanova University, Pennsylvania, PA, USA

HIGHLIGHTS

- Vegetation, N addition, and hydrogeomorphic setting regulate SOM pools in wetlands.
- Interior wetlands store more total SOM and MAOM mass and have lower sand content.
- Creekside soils show greater MAOM stabilization efficiency despite lower SOM.
- N addition enhances MAOM in interior mangroves but reduces it in marsh soils.
- Mangroves favor MAOM stabilization, while marshes retain more C as detrital POM.

GRAPHICAL ABSTRACT

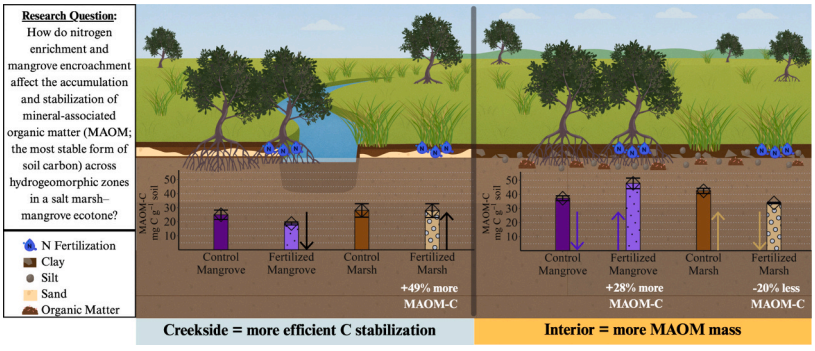

ARTICLE INFO

Keywords:
Marsh-mangrove ecotone
Nutrient pollution
Wetland biogeochemical cycle
Soil organic matter
Organo-minerals
Soil carbon sequestration

ABSTRACT

As average global temperatures rise, coastal wetlands play a crucial role in carbon (C) sequestration and storage, primarily as soil organic matter (SOM). However, the poleward migration of mangroves into salt marsh habitats, along with nitrogen (N) pollution, may alter SOM formation and stability, and thus the capacity of coastal wetlands to preserve soil C long-term. Wetland SOM is composed of mineral-associated organic matter (MAOM), which is considered highly stable due to physicochemical protection, and particulate organic matter (POM), which has a more rapid turnover rate. This study evaluated the effects of mangrove presence, N enrichment, and hydrogeomorphic setting on SOM pools and biogeochemical soil properties in NE Florida, USA, to understand implications for long-term soil C and N preservation. A factorial field experiment (40 plots) tested interactions between hydrogeomorphic location (creekside vs. interior), vegetation (marsh vs. mangrove), and N treatment (fertilized vs. control), across two depths (0–15 and 15–30 cm) on MAOM and POM pools. Interior plots held 58% more MAOM-C and 61% more MAOM-N by mass than creekside plots, with control marshes MAOM-C and MAOM-N exceeding control mangroves. However, when normalized, MAOM accounted for 55.5% of total C and 73.8% of total N in creekside plots, compared to 44.3% and 61.2% in interior plots- suggesting greater C stabilization efficiency. N-fertilization effects varied by vegetation and location. In interior plots (0–15 cm), N-fertilization increased MAOM by 28–30% in mangroves, while decreasing MAOM by 20–21% in marshes. In creekside plots, N-fertilization had no main effect, though fertilized marshes held more MAOM than fertilized

* Corresponding author.
E-mail address: lisa.chambers@ucf.edu (L.G. Chambers).

https://doi.org/10.1016/j.scitotenv.2026.181643
Received 3 May 2025; Received in revised form 27 February 2026; Accepted 1 March 2026
Available online 6 March 2026

mangroves. Collectively, these findings underscore the need for site-specific assessments (vegetation, nutrient inputs, and hydrogeomorphic setting, etc.) of blue C potential as coastal vegetation and nutrient regimes continue to shift.

1. Introduction

Coastal wetlands play a critical role in the global carbon (C) and nitrogen (N) cycles, serving as significant sinks through sediment accretion and soil organic matter (SOM) accumulation (Reddy and Patrick, 1975; Chmura et al., 2003). These ecosystems, including salt marshes and mangroves, contribute to long-term C sequestration (Alongi, 2014; Cahoon et al., 2021) due to low oxygen levels and slow decomposition (Reddy and DeLaune, 2008), while also buffering adjacent waters from nutrient enrichment by retaining and transforming land-derived N (Valiela and Cole, 2002; Hurst et al., 2016). However, the ability of coastal wetlands to function as effective C and N sinks relies on the accumulation and persistence of SOM, which can be sensitive to anthropogenic stressors, including climate change (Ofiti et al., 2023) and nutrient loading (Galloway et al., 2008; Mack et al., 2024).

One of the most recognizable climate-driven changes in temperate and subtropical coastal wetlands is the poleward expansion of mangroves into salt marsh ecosystems as severe winter freeze events become less frequent (Cavanaugh et al., 2014; Saintilan et al., 2014; Chapman et al., 2021; Osland et al., 2013, 2021). Additional drivers include sea-level rise, subsidence, and increased sedimentation (Rogers et al., 2005; Krauss et al., 2011, 2014). In Florida, mangrove cover has increased markedly over recent decades (Rodriguez et al., 2016; Cavanaugh et al., 2019). Studies documented a 69% increase in mangrove abundance in southern portions of the marsh-mangrove ecotone within seven years (Doughty et al., 2016), and northward movement of both *Avicennia germinans* and *Rhizophora mangle* into Georgia (Overstreet et al., 2025; Vervaeke et al., 2025). As mangroves become dominant, they can alter ecosystem structure and services (Kelleway et al., 2017) by 1) replacing herbaceous vegetation with woody trees, 2) modifying C storage (Doughty et al., 2016; Vaughn et al., 2020), and 3) altering sediment dynamics and processes (Coldren et al., 2019; Simpson et al., 2021). Although mangroves contribute substantial organic carbon (OC) inputs to wetland soils due to high aboveground biomass productivity (Doughty et al., 2016; Kelleway et al., 2016), their influence on belowground processing is complex. For example, mangrove roots can introduce oxygen into the soil that may stimulate microbial activity and accelerate organic matter (OM) decay (Barreto et al., 2018). Early work suggests that mangrove encroachment generally enhances soil organic C (SOC) storage (Bianchi et al., 2013; Doughty et al., 2016; Kelleway et al., 2016), yet more recent analyses show that SOC responses are not uniform and depend on environmental setting and time since encroachment (Steinmuller et al., 2022). Together, these findings indicate that the mangrove presence may result in different C pools and fluxes than in salt marsh, expansion are highly context-dependent.

In parallel with shifting vegetation communities, many coastal wetlands have experienced elevated nutrient inputs from agriculture, wastewater, and urbanization over recent decades (Cloern, 2001; Bricker et al., 2008; Galloway et al., 2008). While N and phosphorus (P) inputs occur naturally through weathering and upwelling (Bricker et al., 2008), anthropogenic sources now dominate nutrient delivery to estuaries (CENR, 2000). Resulting eutrophication contributes to harmful algal blooms and episodic wildlife mortality events (Lapointe et al., 2015, 2020; Allen et al., 2022). Although wetlands can retain and transform N (Valiela and Cole, 2002), excessive N input can destabilize wetland soils by reducing biodiversity, accelerating OM decomposition, and reducing root biomass, thereby increasing the risk of subsidence and habitat loss (Deegan et al., 2012; Wigand et al., 2014). Conversely, nutrient additions may also stimulate plant productivity and sediment trapping, potentially increasing resilience to sea-level rise (Morris et al., 2013; Graham and Mendelssohn, 2014; Weaver and Armitage, 2020). These contrasting outcomes highlight the need of understanding how nutrient inputs interact with vegetation type and environmental setting to regulate SOM stability.

Finally, microtopographic and hydrogeomorphic differences within a coastal wetland can influence biogeochemical properties and processing dynamics (Deegan et al., 2007). Creek-adjacent zones, often referred to as 'low marsh', experience frequent inundation, greater tidal flushing, higher mineral sediment deposition, and elevated erosion risk (Wood and Hine, 2007; Fagherazzi and Mariotti, 2012; Sapkota and White, 2019). In contrast, the interior 'high marsh' zones flood less frequently, receive reduced mineral inputs, and accumulate more OM, but may be more prone to peat collapse under stress (Chambers et al., 2019; Hupp et al., 2009). These hydrogeomorphic settings can interact with vegetation type and nutrient status to affect C and N storage and SOM stabilization.

To understand how vegetation, nutrient status, and hydrogeomorphic setting may impact SOM persistence, an understanding of the mechanisms that stabilize SOM is necessary. Recent advances emphasize that SOM persistence reflects microbial processing, mineral interactions, and environmental constraints, rather than intrinsic litter recalcitrance alone (Von Lützow et al., 2007; Kleber, 2010; Schmidt et al., 2011; Castellano et al., 2015; Lehmann and Kleber, 2015; Cotrufo and Lavallee, 2022). Accordingly, SOM is often partitioned into particulate organic matter (POM) and mineral-associated organic matter (MAOM) based on particle size and density (Lavallee et al., 2020; Cotrufo and Lavallee, 2022; Mirabito and Chambers, 2023). The POM pool (>53 μm; <1.6–1.85 g cm^{-3}) consists of larger, high-molecular-weight compounds (including less decomposed plant, microbial fragments), with faster turnover rates (Von Lützow et al., 2007). In contrast, MAOM (<53 μm; >1.6–1.85 g cm^{-3}) forms when smaller, low-molecular-weight compounds and microbial byproducts bind to silt- and clay-sized minerals, which typically exhibit slower cycling and greater physicochemical protection, representing the most stable and persistent form of soil C (Cotrufo et al., 2015; Kleber et al., 2015). The microbial efficiency–matrix stabilization (MEMS) framework posits that labile plant inputs can be efficiently converted into MAOM than more recalcitrant inputs when microbial growth efficiency is high and reactive mineral surfaces are available (Cotrufo et al., 2013). Because mangrove litter often differs from marsh litter in lignin content, N concentrations, and $\delta^{13}C$ signatures (Breithaupt et al., 2019), vegetation type can impact OM lability, and also the balance between POM and MAOM.

Recent work in mangrove soils indicates that POM and MAOM vary in abundance and their contribution to persistent SOM based on the setting. For example, one mangrove study found mineral-associated soil organic C (SOC) fractions to be older and more abundant (34–62%) than low-density fractions (14–44%) (Hamada et al., 2024). Synthesis work similarly suggests that MAOM is more consistently associated with persistent SOC storage where mineral surfaces are abundant, but POM can also persist under strong environmental constraints (e.g., sustained anoxia) (Cooray et al., 2025). Indeed, long-term persistence of POM-rich C has been documented primarily in organic-rich, peat-forming mangrove systems with low mineral inputs and persistent anaerobic conditions (McKee et al., 2007). However, most (~90%) mangrove forests occur in terrigenous sedimentary settings with substantial mineral inputs (Worthington et al., 2020) where organo–mineral interactions are expected to play a more dominant role in SOM stabilization. Furthermore, a recent study in Florida found that MAOM abundance differed by vegetation type, accounting for a larger proportion of SOC in mangrove soils (62%), whereas POM dominated SOC

storage in salt marsh soils (59%) (Assavapanuvat et al., 2024).

Despite widespread changes in marsh vs. mangrove coverage and nutrient enrichment, relatively few studies have examined how vegetation type, nutrient status, and hydrogeomorphic setting interact to regulate MAOM abundance and the balance between POM and MAOM pools in coastal wetlands; rather, most research has focused on bulk C stocks or burial rates (Doughty et al., 2016; Steinmuller et al., 2022). Therefore, a knowledge gap exists in the mechanistic understanding of how SOM fractions differ based on vegetation and N loading, and whether response differs between creekside and interior settings. This study addressed this gap using a factorial field experiment in a mangrove–salt marsh ecotone in northeast Florida, USA. We evaluated N addition in marsh and mangrove plots located in two contrasting hydrogeomorphic settings (creekside vs. interior) and quantified POM- and MAOM-associated C and N, along with soil physicochemical properties and isotopic signatures. The primary objective was to determine how vegetation type, N addition, and hydrogeomorphic setting combine to influence SOM fraction pools and the proportion of total C and N stabilized as MAOM. We hypothesize that: (1) that marsh plots will support greater MAOM formation due to inputs of more labile OM (Cotrufo et al., 2013), whereas mangrove plots will retain a higher proportion of POM due to more recalcitrant inputs (Breithaupt et al., 2019); (2) N addition will enhance MAOM accumulation in mangroves plots through increased belowground inputs and microbial processing, while reducing MAOM formation in marsh plots due to reduced root foraging; and (3) creekside locations will exhibit greater MAOM accumulation than interior plots due to higher mineral sediment inputs that promote stabilization (Fagherazzi and Mariotti, 2012).

2. Methods

2.1. Study site description

This study, part of the WETFEET Project (https://www.wetfeetproject.com/) was conducted within the Guana Tolomato Matanzas National Estuarine Research Reserve (GTMNERR), located along Florida's Atlantic coast near St. Augustine. The GTMNERR receives an annual average precipitation of 1317 mm, while nearby St. Augustine has a mean annual temperature of 20.8 °C (11.1 °C–32.0 °C; (N.O.A.A., 2024). The focal study area, North Matanza (NMAT; Fig. 1C), lies approximately 20 km south of St. Augustine and just north of Matanzas Inlet (29°43′38.3″N, 81°14′25.0″W). Historically, this site marks the northern limit of persistent mangrove presence in the region (Rodriguez et al., 2016), with evidence of mangrove expansion and contraction over the past 250 years (Cavanaugh et al., 2019). Changes in vegetative cover at this site have been documented since at least 1942 via aerial photographs and satellite imagery (Rodriguez et al., 2016). The site experiences a semidiurnal tidal cycle, with two high and two low tides daily, and mean high water of 0.63 m, and a mean low water of −0.65 m relative to NAVD88 (Chapman et al., 2021). The vegetation community reflects the ecotonal nature of the site, featuring C_4 species like *Spartina alterniflora,* (now reclassified as *Sporobolus alterniflorus*; Peterson et al., 2014), and C_3 halophytes such as *Batis maritima* and *Avicennia germinans*. Elevation gradients influence plant distribution: *S. alterniflora* patches dominate the low-elevation creekside areas, while *B. maritima* densities increase further inland. Currently, *A. germinans* is widespread across the landscape, typically growing as low-stature individuals. Site conditions include soil temperatures ranging from 20.8 °C to 30.0 °C, air temperatures from 1.5 °C to 31.0 °C, an elevation of 41 cm above NAVD88, and an average porewater salinity of 39.1‰ (Chapman et al., 2021).

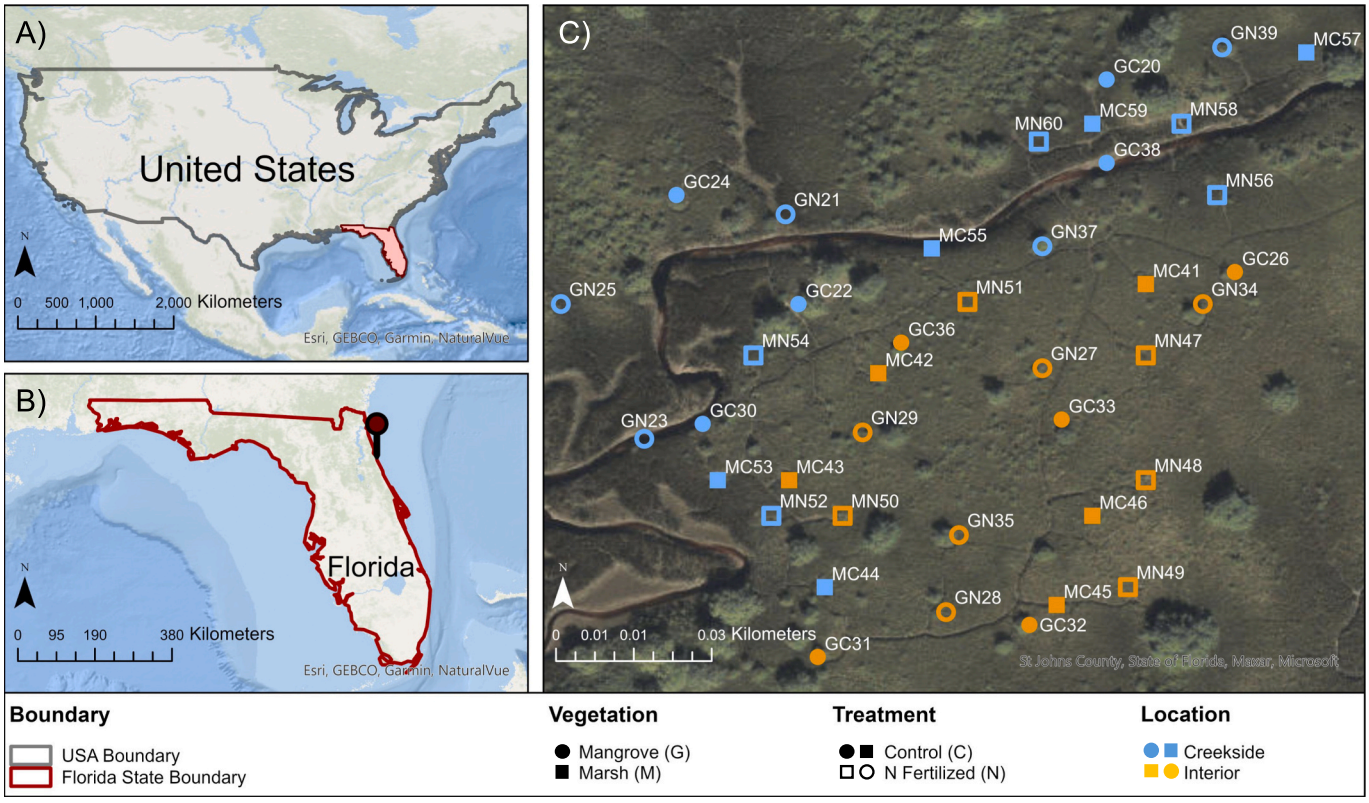

Fig. 1. Study site location and plot distribution. (A) Map of the continental United States showing the location of Florida. (B) Map of Florida highlighting the field site along the northeast coast (red pin). (C) Aerial image of the study area showing the distribution of experimental plots across a salt marsh-mangrove ecotone. Plot symbols indicate vegetation type (circles = mangrove; squares = marsh), nitrogen treatment (filled = control; open = N fertilized), and geomorphic setting (blue = creekside; orange = interior), with five replicates of each combination.

2.2. Experimental design and field sampling

In March 2022, 40 plots (2.25 m^2; 20 creekside, 20 interior) were established at NMAT within a 0.02 km^2 area. Plots followed a full-factorial design: two vegetation types (marsh and mangrove) × two nutrient treatments (N-fertilized and control) × two hydrogeomorphic locations (creekside and interior), with five replicates of each combination (Fig. 1C). This design yielded four distinct plot types (control mangrove, fertilized mangrove, control marsh, and fertilized marsh) in each hydrogeomorphic location (creekside and interior). Mangrove plots contained a single *A. germinans* individual of similar stature (~2 m tall; 4–7 years old), with ages estimated from internode counts (Duarte et al., 1999). These individual mangroves have become established within an existing matrix of marsh, and this study design included only one discrete sampling of "mangrove" and "marsh," rather than documenting the temporal progression of mangrove encroachment into marsh (i.e., there is no baseline or pre-mangrove comparison).

Fertilized plots received 300 g of polymer-coated slow-release urea (46% N) annually in March 2022, April 2023, and May 2024. This application corresponded to 61.3 g N m^{-2} yr^{-1}. Although higher than typical estuarine N loading, this amount was selected to produce a sustained fertilization response in a tidally flushed system and to align with established experimental fertilization rates used near our study site by Dangremond et al. (2020), and originally developed by Feller et al. (2003, 2007). Fertilizer was enclosed in mesh bags and inserted into shallow slits around the plot margins to minimize tidal export and ensure root-zone availability. This application supplemented the site's background nutrient regime, where >90% of floodwater N is in dissolved organic form (GTMNERR SWMP data). "Fertilized" plots were compared to "control" (unfertilized) plots with one discrete measurement to determine the outcome after two years of nutrient enrichment; changes over time or from a known baseline were not quantified. The hydrogeomorphic classification was based on proximity to the tidal creek: plots within 3 m of the creek were designated "creekside," while those located more than 3 m away were "interior.".

In March 2024, intact soil cores (7 cm diameter × 30 cm depth) were collected from each plot using an acrylic push-core method to minimize compaction (Upreti, 2019). These samples were taken after two years of fertilization (March 2022 and April 2023) and immediately prior to the third application in May 2024. Sampling was consistently performed on the same side of each plot (facing the plot front) to ensure consistency. In the field, each core was sectioned into 0–15 cm and 15–30 cm soil intervals, placed in Ziploc bags, and transported on ice to the Aquatic Biogeochemistry Laboratory (ABL) at the University of Central Florida (UCF). In the lab, samples were weighed, homogenized, and stored at 4 °C until further analysis.

2.3. Soil physicochemical properties and nutrients

The soil physicochemical properties analyzed for 0–15 and 15–30 cm soil depths included moisture content, bulk density, pH, percent OM, total carbon (TC), total nitrogen (TN), total phosphorus (TP), and particle size analysis. Gravimetric moisture content was calculated by weighing homogenized soil subsamples before and after drying at 70 °C until a constant weight was achieved. Bulk density was determined based on the wet weight of a known soil volume and moisture content. Soil pH was measured by creating a 1:5 soil-to-water slurry using ~5 g of soil and 25 mL of nanopure water. After stirring and allowing the slurry to sit for 30 min, pH was measured with an Accumet XL200 benchtop pH probe (Thermo Fisher Scientific), as described by Thomas 1996 (with modifications). Oven dried soil subsamples were finely ground in a SPEX 8000 M Mixer/Mill (SPEX Sample Prep, Metuchen, NJ, USA). The homogenized, dried, and ground soil subsamples were analyzed for TC and TN using a Vario Micro Cube CN Analyzer (Elementar Americas Inc., Mount Laurel, NJ, USA). Method detection limits of 0.07 g C kg^{-1} and 0.005 g N kg^{-1}. Analytical precision, assessed using replicate measurements, was within 2–9% relative standard deviation (RSD). Accuracy was verified through repeated analysis of certified reference materials, with recovery ranging from 97 to 103%. Total P was measured following the ashing-digestion method outlined by Andersen (1976). Approximately 0.3 g of dried, ground soil subsamples were placed in 50 mL digestion tubes and ashed at 550 °C for 4 h in a muffle furnace. Loss on ignition was used to determine % OM by comparing the ashed weight to the pre-burn dry weight (Sparks et al., 1996). After combustion, the samples were moistened with deionized (DI) water and dissolved in 50 mL of 1 M HCl. The digestion tubes were placed on a digestion block at 100–120 °C per 30 min. The samples were cooled, filtered through Whatman #41 filter paper, and diluted to volume with DI water in 50 mL volumetric flasks. The TP of the digests was determined colorimetrically using a SEAL AQ2 Automated Discrete Analyzer (SEAL Analytical Inc., Mequon, Wisconsin) in accordance with U.S. EPA method 365.1 Rev.2 with a detection level 0.001 mg P L^{-1} (RSD = 1–2%; recovery = 100–110%).

Particle size analysis was conducted using oven-dried soil samples. Approximately 2 g of ground soil was weighed into a crucible and ashed in a muffle furnace at 550 °C for 4 h to remove OM. Around 1 g of ashed soil was transferred to a centrifuge tube and 40 mL of 4% sodium hexametaphosphate was added as a dispersant. The mixture was vortexed briefly, then shaken on an orbital shaker at 150 RPM for 24 h. Particle size distribution was measured using a Cilas 1190 Particle Size Analyzer (Cilas, Orléans, France) to quantify clay, silt, and sand fractions, classified according to USDA standards (<0.02 μm for clay, 0.02–0.50 μm for silt, and > 50 μm for sand; USDA NRCS, 2011) (RSD = 1–10%). The final composition was normalized so that SOM, clay, silt, and sand collectively totaled 100% (Fig. 2).

Extractable ammonium (NH_4^+), nitrate (NO_3^-), soluble reactive phosphorus (SRP), and dissolved organic carbon (DOC) were measured within 48 h after soil collection. Approximately 5 g of homogenized, field-moist soil subsamples were placed in 40 mL centrifuge tubes, then 20 mL of 2 M KCl was added. The mixtures were shaken on a longitudinal shaker for 1 h, then centrifuged at 4000 *g* for 10 min at 10 °C using a Sorvall RC 5C Plus centrifuge (Weaverville, NC). The supernatants were vacuum filtered through 0.45 μm membrane filters, acidified with concentrated H_2SO_4 for preservation, and refrigerated at 4 °C until analysis. The samples were analyzed using a SEAL AQ2 Automated Discrete Analyzer (Seal Analytical), with detection limits of 0.006 mg NO_3-N L^{-1} (RSD = 1–15%; recovery = 95–120%), 0.007 mg NH_4-N L^{-1} (RSD = 1–15%; recovery = 95–110%), and 0.002 mg P L^{-1} (RSD = 1–2%; recovery = 100–120%), according to EPA methods 231-A Rev.0, 210-A. Rev. 1, and 204-A Rev. 0, respectively (USEPA, 1993). DOC was determined using a TOC-L Analyzer (Shimadzu Scientific Instruments, Kyoto, Japan) (RSD = 2–20%; recovery = 95–115%).

2.4. Soil fractionation

The MAOM and POM were isolated using a combination of physical and density fractionation, following the protocol of Mirabito and Chambers (2023). For physical fractionation, ~15 g of dry-equivalent, field-moist soil was dispersed in a 0.5% sodium hexametaphosphate solution (1:8 soil-to-solution ratio) and shaken for 18 h to disrupt aggregates and release occluded OM (Cambardella and Elliott, 1992). The resulting slurry was wet-sieved through a 53 μm mesh to separate coarse (>53 μm) from fine (<53 μm) particles. Material retained on the sieve was backwashed into pre-weighed containers and dried at 70 °C to constant weight. The >53 μm fraction was classified as POM, while a ~1 g subsample of the <53 μm fraction was subjected to density separation using 20 mL of sodium polytungstate (density 1.85 g cm^{-3}). Samples were shaken at 150 RPM for 18 h, centrifuged at 3400 RPM (20 °C) for 30 min, and the floating light fraction (LF; POM; <1.85 g/cm^3) was aspirated, filtered, rinsed, and dried, and was classified as POM. The remaining heavy fraction (HF; MAOM; >1.85 g/cm^3) was rinsed thoroughly, centrifuged at 5000 RPM for 10 min to remove salts, dried at

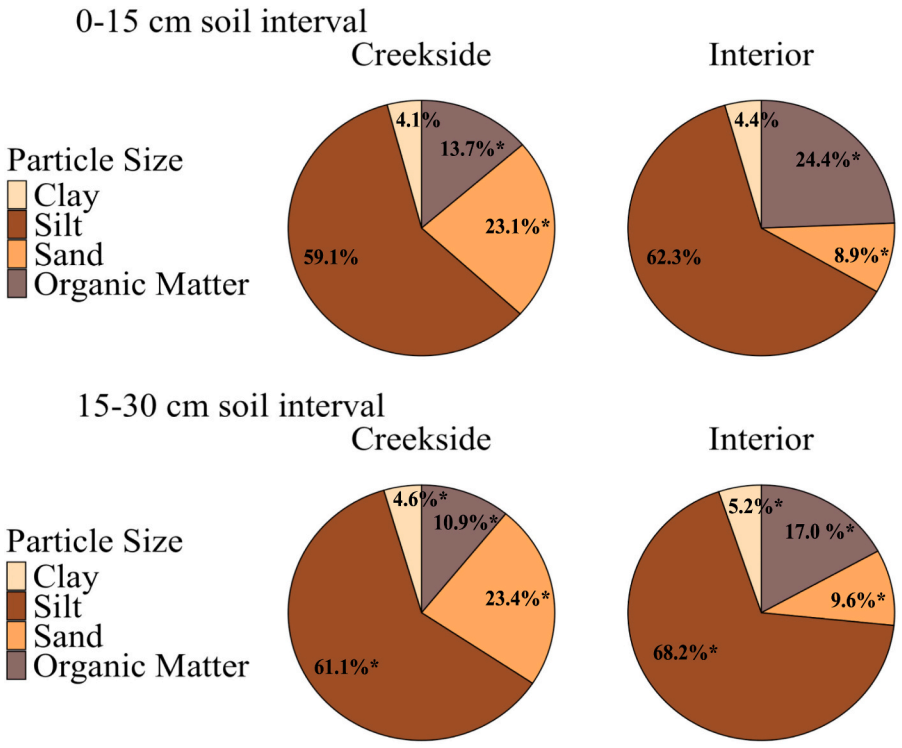

Fig. 2. Soil particle size and organic matter composition (% by mass) by depth and location. Asterisks indicate statistical differences across locations within each depth ($n = 20$; $p < 0.05$).

70 °C, and classified as MAOM. The final POM pool comprised the LF material isolated during density separation, combined with the coarse >53 μm OM from physical fractionation. Both POM and MAOM fractions were ground and analyzed for total C and N using a Vario Micro Cube CN Analyzer (Elementar Americas Inc., Mount Laurel, NJ, USA) (RSD = 2–6%; recovery = 95–105%).

2.5. Stable isotope analysis

Stable isotope analysis was conducted to determine the $\delta^{13}C$ composition of the POM and MAOM fractions. Dried and ground subsamples from both fractions were processed at the Stable Isotope Mass Spectrometry Laboratory, Department of Geological Sciences, University of Florida. The laboratory processed the samples and provided $\delta^{13}C$ values. Analyses were performed using a Costech ECS 4010 Elemental Combustion System coupled to an isotope ratio mass spectrometer (RSD = 0–0.2‰). Isotope ratios were reported in delta (δ) notation relative to the Vienna Pee Dee Belemnite (VPDB) standard, and also expressed as atom % ^{13}C.

2.6. Data analysis

All statistical analyses were conducted in R version 4.0.3 within RStudio (R Foundation for Statistical Computing, Vienna, Austria; RStudio Inc., Boston, MA, USA). Data visualization was performed using the "ggplot"2 package (Wickham, 2016), and data processing employed tidyverse (Wickham et al., 2019). Outliers were assessed using the generalized ESD test from the "envStats" package and by visual inspection of boxplots (Millard and Kowarik, 2025). Normality was evaluated with the Shapiro-Wilk test (α = 0.05) and normal Q-Q plots, while Levene's test (α = 0.05) was used to assess the homogeneity of variances. When assumptions for parametric ANOVA were not met—even after transformation—generalized linear models (GLMs) or generalized linear mixed models (GLMMs) were applied, using either the Gaussian or Gamma distribution with a log link. Model selection was guided by Akaike Information Criterion (AIC) scores using the "AICcmodavg" package (Mazerolle, 2020), with residual plots used to further validate model fit. The "performance" package (Lüdecke et al., 2021) was used to assess model assumptions including normality, variance homogeneity, and collinearity, while "DHARMa" package (Hartig and Lohse, 2022) was used to evaluate residual diagnostics for GLMs or GLMMs. Adjusted R^2 values were estimated with the "MuMIn" package (Barton, 2023). Pairwise comparisons between vegetation and treatment were evaluated using Tukey's HSD post hoc test within the "emmeans" package (Lenth, 2020).

To answer the research questions, data were subset by soil depth (0–15 cm and 15–30 cm). Fractionated SOM pools (MAOM and POM) were analyzed using GLMMs with interaction terms for vegetation type (marsh vs. mangrove), treatment (N fertilized vs. control), and location (creekside vs. interior) as fixed effects, and plotID as a random effect to account for repeated measures across plots (model: mg.C.g.soil ~ vegetation*treatment*location + (1|plotID), family = Gamma(link = "log")). Results were reported as means ± standard error ($N = 5$). If no significant interaction or main effects were found (α = 0.05) between vegetation and treatment, data were pooled by location ($N = 20$). Soil physicochemical properties were analyzed using three-way ANOVAs (model: ~ vegetation * treatment * location), with exceptions for extractable NH_4^+ and DOC (0–15 cm), and for TC, NH_4^+, and NO_3^- (15–30 cm), which were analyzed using Gamma-distributed GLMs. Soil particle size data were analyzed using a Gamma GLMM with vegetation, treatment, and location as the fixed predictors. $\delta^{13}C$ isotope values in the MAOM fraction were analyzed with three-way ANOVA by vegetation*treatment*location. Principal components analysis (PCA) was performed using the "ggfortify" and "FactoMineR" packages (Tang et al., 2016; Lê et al., 2008). C content in MAOM and POM fractions was calculated both as mg C per gram of soil, reflecting total pool size, and mg C per gram of total C (%) providing insight into the proportion of stabilized OM relative to the total. All analytical measurements were performed following standard laboratory QA/QC protocols, and reported values reflect the analytical precision of each method.

3. Results

3.1. General soil properties and phosphorus

Across all depths, TP, pH, and the C:N ratio did not differ by location (creekside vs. interior), vegetation (marsh vs. mangrove), or treatment (N fertilized vs. control) ($p > 0.065$). Location strongly influenced most soil physicochemical properties. At 0–15 cm, interior plots had 24% higher moisture content ($p < 0.001$), 39% lower bulk density ($p < 0.001$), and 78% more OM ($p < 0.001$) than creekside plots. Similar trends were observed at 15–30 cm: interior plots had 16% higher moisture ($p = 0.017$), 24% lower bulk density ($p = 0.008$), 56% more OM ($p = 0.001$; Table 1). Particle size distribution also differed by location. At 0–15 cm, sand content was 61% lower in the interior plots (8.91 ± 1.03%) compared to the creekside plots (23.1 ± 3.72%; $p < 0.001$), while silt and clay content did not differ ($p > 0.275$; Fig. 2). At 15–30 cm, sand was 59% lower, silt 12% higher, and clay 13% higher in interior plots than creekside plots ($p < 0.001$; $p = 0.017$; $p = 0.039$; Fig. 2). Moisture content, bulk density, OM, and particle size distribution did not differ by vegetation or treatment ($p > 0.262$).

3.2. Soil carbon fractions

The main effect of location influenced the greatest number of C pool properties. Total C averaged 65% higher in interior plots than creekside plots at 0–15 cm ($p < 0.001$) and 32% higher at 15–30 cm ($p = 0.046$; Table 1). No differences in TC were observed by vegetation or treatment ($p > 0.262$). Dissolved organic carbon (DOC) followed the same spatial pattern, with concentrations 115% higher in the interior at 0–15 cm (132 ± 13.4 vs. 61.6 ± 7.98 mg kg^{-1}; $p < 0.001$) and 82% higher at 15–30 cm (83.7 ± 9.42 vs. 46.0 ± 4.01 mg kg^{-1}; $p < 0.001$) than creekside plots. Among the physicochemical fractions, POM-C mass dominated SOM in interior plots (mean of 54–56%), while MAOM-C mass was the dominant form of SOM in creekside plots (53–58%). At 0–15 cm, interior plots contained 131% more POM-C than creekside plots (52.5 ± 2.70 vs. 22.7 ± 2.98 mg C g^{-1} soil; $p < 0.001$). At 15–30 cm, POM-C was 86% higher in interior plots (28.0 ± 2.75 vs. 15.0 ± 2.41 mg C g^{-1} soil; $p < 0.001$). The mass of stable C (as MAOM-C) showed similar trends. At 0–15 cm, interior plots contained 58% greater MAOM-C than creekside plots (41.2 ± 1.64 vs. 26.0 ± 2.09 mg C g^{-1} soil; $p < 0.001$), and 17% greater at 15–30 cm, though the latter was not statistically different ($p = 0.193$). However, when viewed as a percentage of TC, a larger proportion of TC was stabilized as MAOM-C in the creekside plots. MAOM-C comprised 55.5 ± 2.0% of TC in creekside plots, compared to 44.3 ± 1.5% in interior plots at 0–15 cm ($p < 0.001$), and 58.4 ± 2.1% vs. 47.7 ± 1.4% at 15–30 cm ($p < 0.001$).

Vegetation and treatment interaction were most pronounced for DOC and surface SOM fractions. In the interior at 0–15 cm, DOC in the fertilized mashes was nearly twice as high as in fertilized mangroves (199 ± 33.8 vs. 104 ± 10.5 mg kg^{-1}; $p = 0.001$); and fertilized marshes also averaged 38% more DOC than control marshes (132 ± 14.4 mg kg^{-1}; $p = 0.029$). In creekside plots at 0–15 cm, DOC was more than double in fertilized marshes relative to fertilized mangroves (78.4 ± 23.1 vs. 37.7 ± 7.43 mg kg^{-1}; $p = 0.008$; Fig. 5A).

For the physicochemical fractions, marshes tended to hold more POM-C than mangroves in the surface soil. In the interior control plots, marshes had 31% more POM-C than mangroves (57.9 ± 5.47 vs. 44.3 ± 2.73 mg C g^{-1} soil; $p = 0.037$). In the creekside fertilized plots, marshes had 49% more POM-C than mangroves (25.6 ± 7.03 vs. 12.8 ± 0.58 mg C g^{-1} soil; $p = 0.033$; Fig. 3A; Table S1). At 15–30 cm, vegetation did not affect POM-C mass at either location ($p > 0.102$; Fig. 4A; Table S1).

MAOM-C also varied by vegetation at the surface soil. In the interior control plots, marshes held 14% more MAOM-C than mangroves (42.5 ± 1.85 vs. 37.3 ± 1.69 mg C g^{-1} soil; $p = 0.049$), while in the fertilized plots, marshes had 29% less MAOM-C than mangroves (33.9 ± 0.51 vs. 47.9 ± 3.76 mg C g^{-1} soil; $p < 0.001$). In creekside plots, the trend was reversed: in the fertilized plots, marshes contained 49% more MAOM-C than mangroves (27.9 ± 4.91 vs. 18.8 ± 1.05 mg C g^{-1} soil; $p = 0.037$; Fig. 3A; Table S1). At 15–30 cm, MAOM-C did not differ by vegetation or treatment at either location ($p > 0.102$; Fig. 4A). When viewed as a percentage of TC, at 0–15 cm in the interior fertilized plots, MAOM-C comprised 49.9 ± 2.86% of TC in mangroves, compared to 41.4 ± 2.87% in marshes ($p = 0.033$; Table S2), mirroring the pattern observed for MAOM-C mass per gram of soil. No vegetation or treatment differences were observed between surface interior control plots ($p > 0.877$) or in creekside plots at either depth ($p > 0.202$).

The treatment interaction effects also influenced some C pools. At 15–30 cm in the interior mangroves, POM-C was 66% higher in fertilized than controls (33.1 ± 6.01 vs. 20.0 ± 4.19 mg C g^{-1} soil; $p = 0.038$; Fig. 4A; Table S1). No treatment effects were observed in creekside POM-C at both depths ($p > 0.4366$). However, MAOM-C mass strongly varied by treatment at surface soil. In the interior fertilized mangroves plots held 28% more MAOM-C than controls ($p < 0.001$), while in the fertilized marshes plots held 20% less than their controls ($p = 0.001$; Fig. 3A). No treatment-related differences were observed in the deeper interior soils or in the creekside plots at either depth. Regarding stabilization efficiency (i.e., percentage of TC as MAOM-C), at 15–30 cm in the interior mangroves, MAOM-C comprised 53.5 ± 3.29% of TC in control plots, compared to 44.7 ± 3.15% in fertilized plots ($p = 0.001$; Table S2); no other treatment-related differences were observed.

3.3. Soil nitrogen fraction

The main effect of location also influenced the greatest number of N pool properties. At 0–15 cm, interior plots had 72% more TN than creekside plots ($p < 0.001$), while at 15–30 cm, the difference was not statistically significant ($p = 0.065$; Table 1). Among extractable N pools, NH_4^+ concentrations were 146% higher in interior plots than creekside plots at 0–15 cm (3.35 ± 0.32 vs. 1.36 ± 0.23 mg kg^{-1}; $p < 0.001$) and 45% higher at 15–30 cm (1.39 ± 0.14 vs. 0.96 ± 0.20 mg kg^{-1}; $p = 0.017$). The physicochemical fractions of N followed the same trend as the C fractions– both POM-N and MAOM-N mass were higher in interior

Table 1
Average sediment/soil physicochemical properties (mean ± standard error, $n = 20$) were determined from homogenized samples collected at each location and depth. $\delta^{13}C$ composition were determined in MAOM and POM fractionated soil. Different letters indicate significant differences across locations within each soil property and depth ($p < 0.05$); b.d. indicates below detection.

	0–15 cm soil interval		15–30 cm soil interval	
	Creekside	Interior	Creekside	Interior
Moisture content (%)	56.7 ± 2.33^b	70.3 ± 0.67^a	50.6 ± 2.86^b	58.6 ± 1.90^a
Bulk density (g cm^{-3})	0.58 ± 0.04^a	0.35 ± 0.01^b	0.71 ± 0.05^a	0.54 ± 0.03^b
Organic matter (%)	13.7 ± 1.52^b	24.4 ± 0.73^a	10.9 ± 1.36^b	17.0 ± 0.96^a
Total phosphorus (mg kg^{-1})	338 ± 37.5^a	391 ± 18.9^a	189 ± 25.5^a	204 ± 15.1^a
Total carbon (g kg^{-1})	51.3 ± 5.35^b	84.8 ± 2.86^a	37.3 ± 4.86^b	49.3 ± 3.74^a
Total nitrogen (g kg^{-1})	3.20 ± 0.33^b	5.51 ± 0.18^a	2.11 ± 0.31^a	2.81 ± 0.22^a
C:N ratio	16.2 ± 0.38^a	15.4 ± 0.23^a	19.0 ± 0.73^a	17.7 ± 0.28^a
Extractable NO_3^- (mg kg^{-1})	0.32 ± 0.04^b	0.49 ± 0.04^a	0.20 ± 0.03^a	0.26 ± 0.02^a
Extractable PO_4^- (mg kg^{-1})	b.d	b.d	0.07 ± 0.05	b.d
pH	5.45 ± 0.24^a	5.50 ± 0.13^a	5.37 ± 0.18^a	5.60 ± 0.08^a
δ^{13}C-MAOM (‰)	−23.8 ± 0.24^a	−24.7 ± 0.18^b	−23.5 ± 0.38^a	−23.8 ± 0.22^a
δ^{13}C-POM (‰)	−22.1 ± 0.57^a	−22.8 ± 0.29^a	−21.6 ± 0.55^a	−21.4 ± 0.32^a

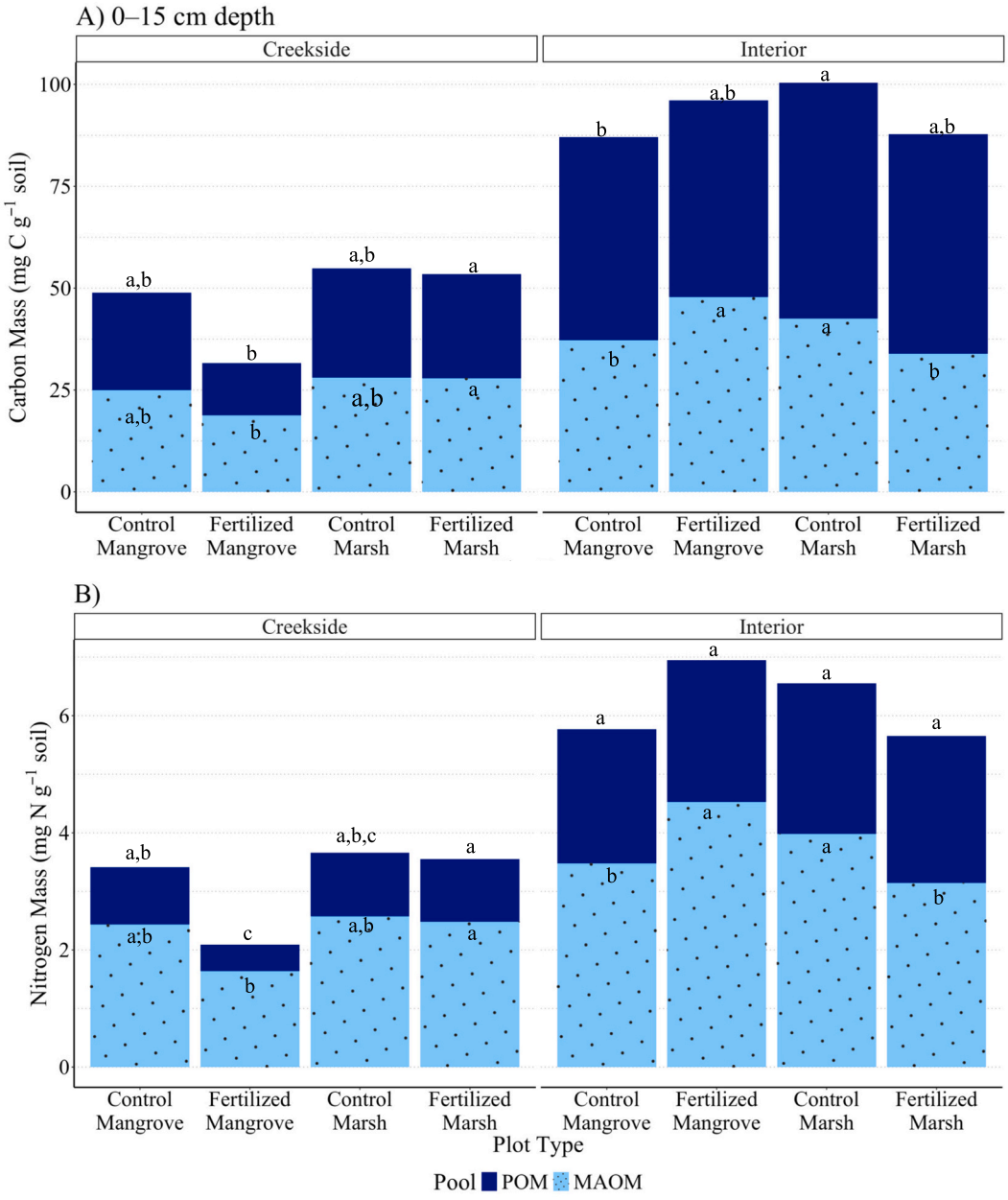

Fig. 3. The concentration of A) Carbon and B) Nitrogen per total gram of soil in the MAOM and POM pool for all four plot types across the interior and creekside locations in the 0–15 cm depth. Bar plots display the means ($n = 5$, $p < 0.05$). Different letters denote significant differences ($p < 0.05$) across plot types within the same location and pool.

plots. Also, MAOM-N mass was the dominant pool at both locations, comprising 61–66% in interior plots and 72–74% in creekside plots. At 0–15 cm, POM-N averaged 164% higher in interior plots (2.45 ± 0.12 vs. 0.93 ± 0.14 mg N g^{-1} soil; $p < 0.001$), and 66% higher at 15–30 cm (1.06 ± 0.13 vs. 0.64 ± 0.12 mg N g^{-1} soil; $p < 0.001$). MAOM-N showed similar patterns. At 0–15 cm, interior plots held 61% more MAOM-N than creekside plots (3.86 ± 0.15 vs. 2.39 ± 1.21 mg N g^{-1} soil; $p < 0.001$), and 16% more at 15–30 cm (2.08 ± 0.15 vs. 1.80 ± 0.22 mg N g^{-1} soil; $p = 0.294$). However, a larger proportion of TN was stabilized as MAOM-N in the creekside plots. MAOM-N comprised 73.8 ± 1.7% of TN in creekside plots, compared to 61.2 ± 1.2% in interior plots at 0–15 cm ($p < 0.001$), and 74.2 ± 1.5% vs. 67.9 ± 1.5% at 15–30 cm ($p = 0.003$).

Vegetation interaction effects were most apparent in the 0–15 cm surface layer. NH_4^+ in fertilized plots was nearly double in marshes (2.16 ± 0.54) compared to mangroves (1.04 ± 0.48; $p = 0.035$); and for the control plots, NH_4^+ was also higher in marshes (1.64 ± 0.20) than mangroves (0.58 ± 0.15; $p = 0.003$; Fig. 5B). POM-N was more variable, at 0–15 cm, no differences were found between interior mangroves and marshes at both fertilized and control plots ($p = 0.369$), but in fertilized creekside plots, marshes contained 138% more POM-N than mangroves (1.07 ± 0.33 vs. 0.45 ± 0.02 mg N g^{-1} soil; $p = 0.016$; Fig. 3B; Table S1). No vegetation differences were observed at 15–30 cm in either location ($p = 0.095$; Fig. 4B). MAOM-N mass followed the same trend as MAOM-C mass in the surface layer. In the interior control plots, marshes contained 14% more MAOM-N than mangroves (3.98 ± 0.15 vs. 3.48 ± 0.12 mg N g^{-1} soil; $p = 0.027$), while in the fertilized plots, marshes had 31% less MAOM-N than mangroves (3.14 ± 0.08 vs. 4.53 ± 0.34 mg N g^{-1} soil; $p < 0.001$; Fig. 3B). In the creekside the trend was the opposite again, in the fertilized plots, marshes contained 51% more MAOM-N than mangroves (2.48 ± 0.44 vs. 1.64 ± 0.15 mg N g^{-1} soil; $p = 0.045$). No vegetation effects were observed at 15–30 cm at both

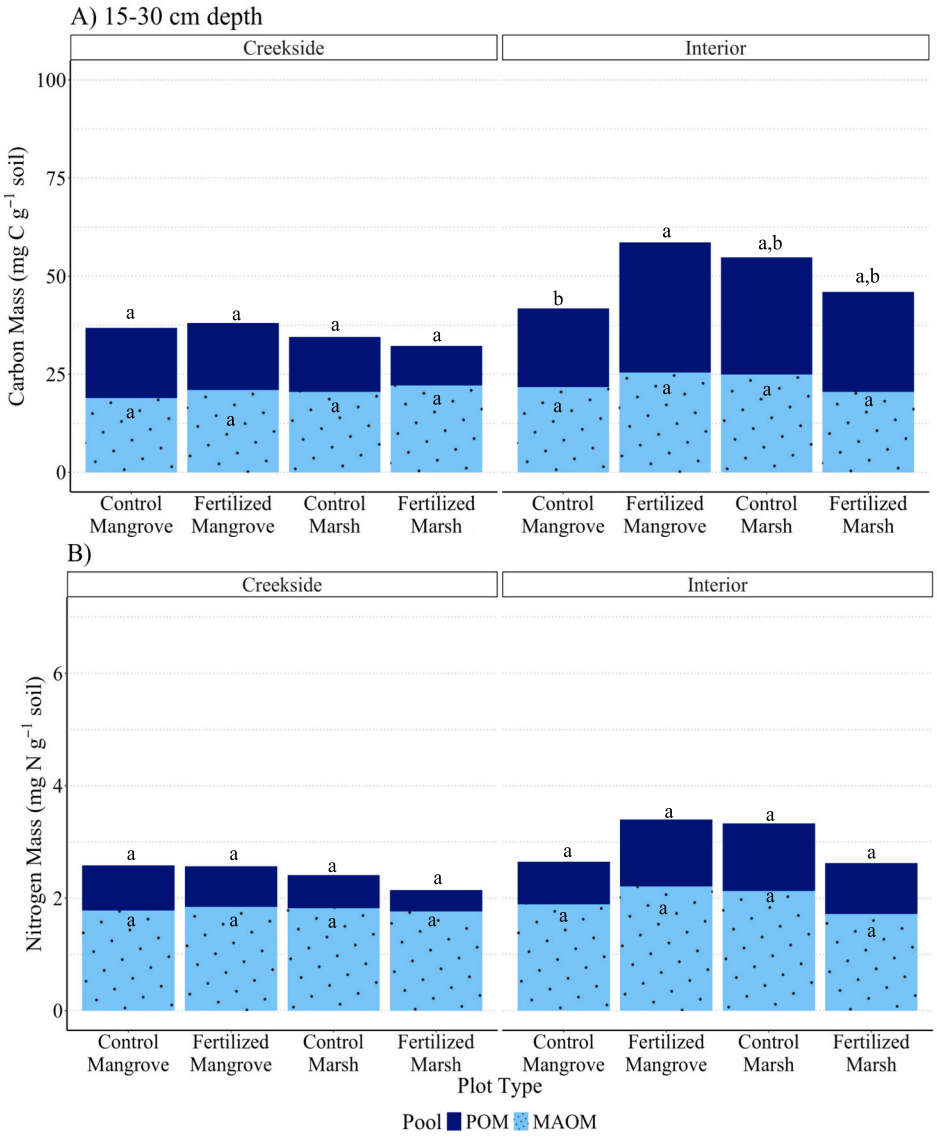

Fig. 4. The concentration of A) Carbon and B) Nitrogen per total gram of soil in the MAOM and POM pool for all four plot types across the interior and creekside locations in the 15–30 cm depth. Bar plots display the means (n = 5; p < 0.05). Different letters denote significant differences (p < 0.05) across plot types within the same location and pool.

locations ($p > 0.102$; Fig. 4B). When viewed as a percentage of TN, at 0–15 cm in the interior fertilized plots, MAOM-N comprised 65.3 ± 2.3% of TN in mangroves, compared to 58.1 ± 2.4% in marshes ($p = 0.028$; Table S2), consistent with trends observed in MAOM-N per gram of soil. No vegetation-related differences were observed between interior control plots ($p > 0.877$) or in creekside plots at either depth ($p > 0.202$).

Treatment interaction effects was stronger for extractable NH_4^+ and MAOM-N fractions. At 0–15 cm in the interior mangroves, NH_4^+ increased by ~80% from control to fertilized plots (2.19 ± 0.21 to 3.93 ± 0.81 mg kg^{-1}; $p = 0.003$), while marsh plots showed no significant treatment response ($p > 0.109$) (Fig. 5B). POM-N mass was less variable by treatment, with only creekside mangroves at 0–15 cm exhibiting higher N concentration in the control plots compared to fertilized plots (0.98 ± 0.20 vs. 0.45 ± 0.02 mg N g^{-1} soil; $p = 0.030$; Fig. 3B). However, MAOM-N followed the same trend as MAOM-C. At 0–15 cm in the interior mangroves, fertilized plots had 30% more MAOM-N than controls (4.53 ± 0.34 vs. 3.48 ± 0.12 mg N g^{-1} soil; $p < 0.001$), while in the marshes, fertilized plots had 21% less than their controls (3.14 ± 0.08 vs. 3.98 ± 0.15 mg N g^{-1} soil; $p < 0.001$; Fig. 3B). No treatment interaction effects were observed for MAOM-N in deeper interior soil and in the creekside at both depths ($p > 0.784$). When normalized to TN, MAOM-N per g N did not differ by treatment at both location and depths (Table S2).

3.4. $\delta^{13}C$ and PCA analysis

At 0–15 cm, MAOM $\delta^{13}C$ was more negative in interior plots than in creekside ($p = 0.006$). POM $\delta^{13}C$ was less depleted and similar between locations, with no statistical difference detected ($p = 0.297$). No differences in MAOM or POM $\delta^{13}C$ were detected at 15–30 cm ($p > 0.532$; Table 1). The PCA of MAOM-related variables revealed distinct clustering by location, with interior plots (orange) separating from creekside plots (blue) along PC1, which explained 59.8% of total variation. Interior plots were associated with variables promoting MAOM formation, including higher OM, moisture, clay, silt, TC, TN, and ammonium concentrations. In contrast, creekside plots aligned with higher sand content, bulk density, and C:N ratio (Fig. 6).

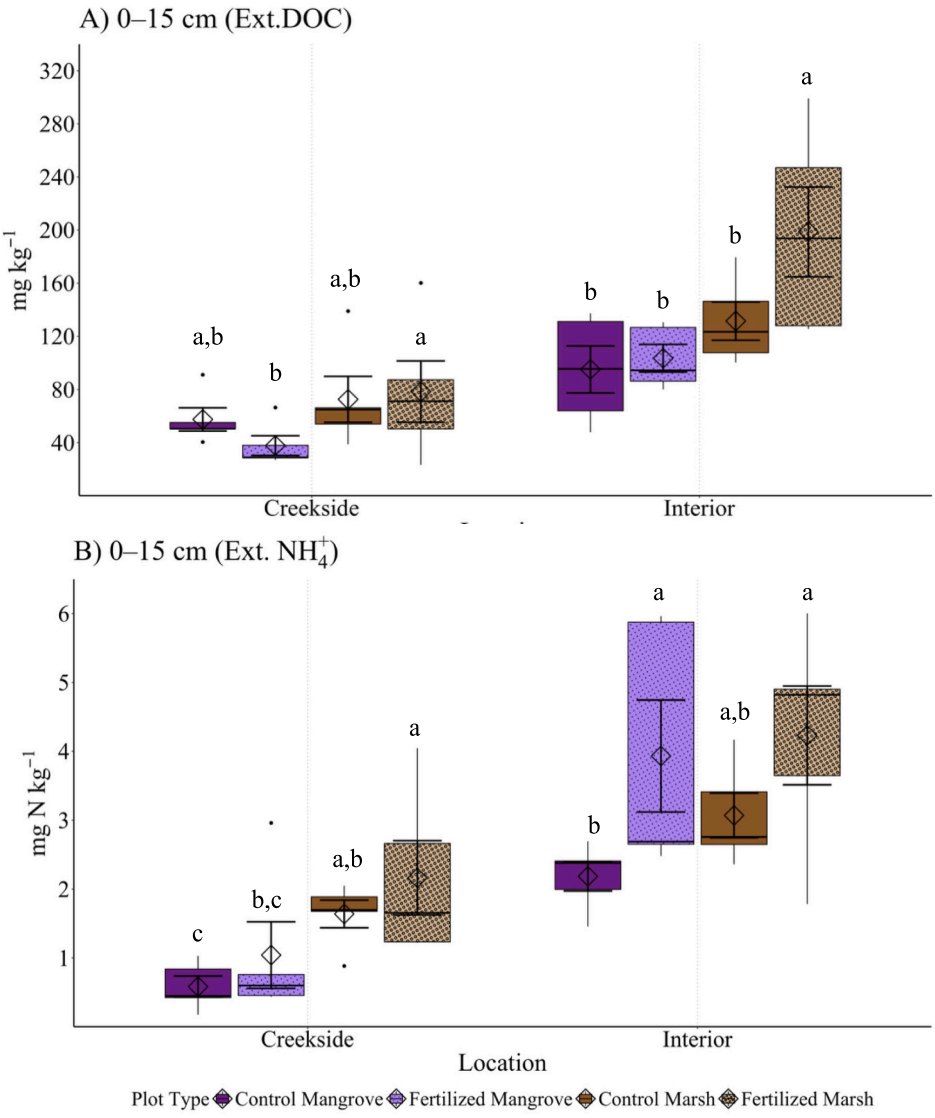

Fig. 5. Extractable nutrient concentrations (mg kg^{-1}) at 0–15 cm depth for (A) dissolved organic carbon (DOC) and (B) ammonium (NH_4^+) across locations and plot types. Different letters indicate significant differences across plot types within the same location ($p < 0.05$, $n = 5$).

4. Discussion

4.1. Greater MAOM accumulation in interior vs. creekside

The substantially greater accumulation of MAOM-C and MAOM-N mass in interior plots, relative to creekside plots, likely reflects more favorable conditions for organo-mineral association. This includes higher soil moisture, lower bulk density, lower sand content, and greater OM, TC, and TN observed in interior plots, all of which may enhance organo-mineral interactions (Kleber et al., 2015; Lavallee et al., 2020; Lewis et al., 2021; Fig. 2). The PCA results (Section 3.4; Fig. 6) further support the clustering of interior plots with variables the include OM, TC, TN, moisture, fine texture, and NH_4^+; meanwhile creekside plots are associated with higher sand content, higher bulk density, and C:N ratios—conditions less favorable for MAOM formation.

Hydrologic differences are likely a key abiotic driver of these physicochemical differences seen based on location. Interior plots, located at a slightly higher elevation (Bravo et al., in review) and farther from tidal creeks, experience reduced tidal flushing that encourages autochthonous OM accumulation, whereas creekside plots are frequently inundated, enhancing export and exchange (Fagherazzi and Mariotti, 2012) of both particulate and dissolved OM. The $\delta^{13}C$ values also support this interpretation: interior MAOM was more depleted (−24.68‰), consistent with C_3 plant inputs (e.g., *A. germinans* and *B. maritima*), while creekside $\delta^{13}C$ signatures (−23.80‰) suggested a greater influence of microbial-processed or marine-derived C (Bouillon et al., 2008; Kristensen et al., 2008; Table 1).

Although interior plots contained more MAOM mass overall, creekside plots had a higher proportion of their TC and TN stabilized as MAOM. This indicates higher stabilization efficiency despite lower total OM. While this highlights a spatial trade-off between OM accumulation and stabilization efficiency, it is important to consider that creekside zones typically occupy a smaller proportion of the landscape. Therefore, interior wetlands, despite lower stabilization efficiency, are likely to contribute more to total MAOM storage at the ecosystem scale. The POM pool was also over twice as high in interior plots, both in mass and percentage, indicating better retention of free (unassociated) SOM inputs under the low-energy conditions and suggesting POM losses during tidal exchange in creekside locations. Together, these patterns emphasize the need to account for both hydrogeomorphic setting and stabilization efficiency when assessing soil C dynamics in coastal wetlands. It also highlights how both POM and MAOM fractions can contribute to SOC persistence under different physical and hydrologic regimes.

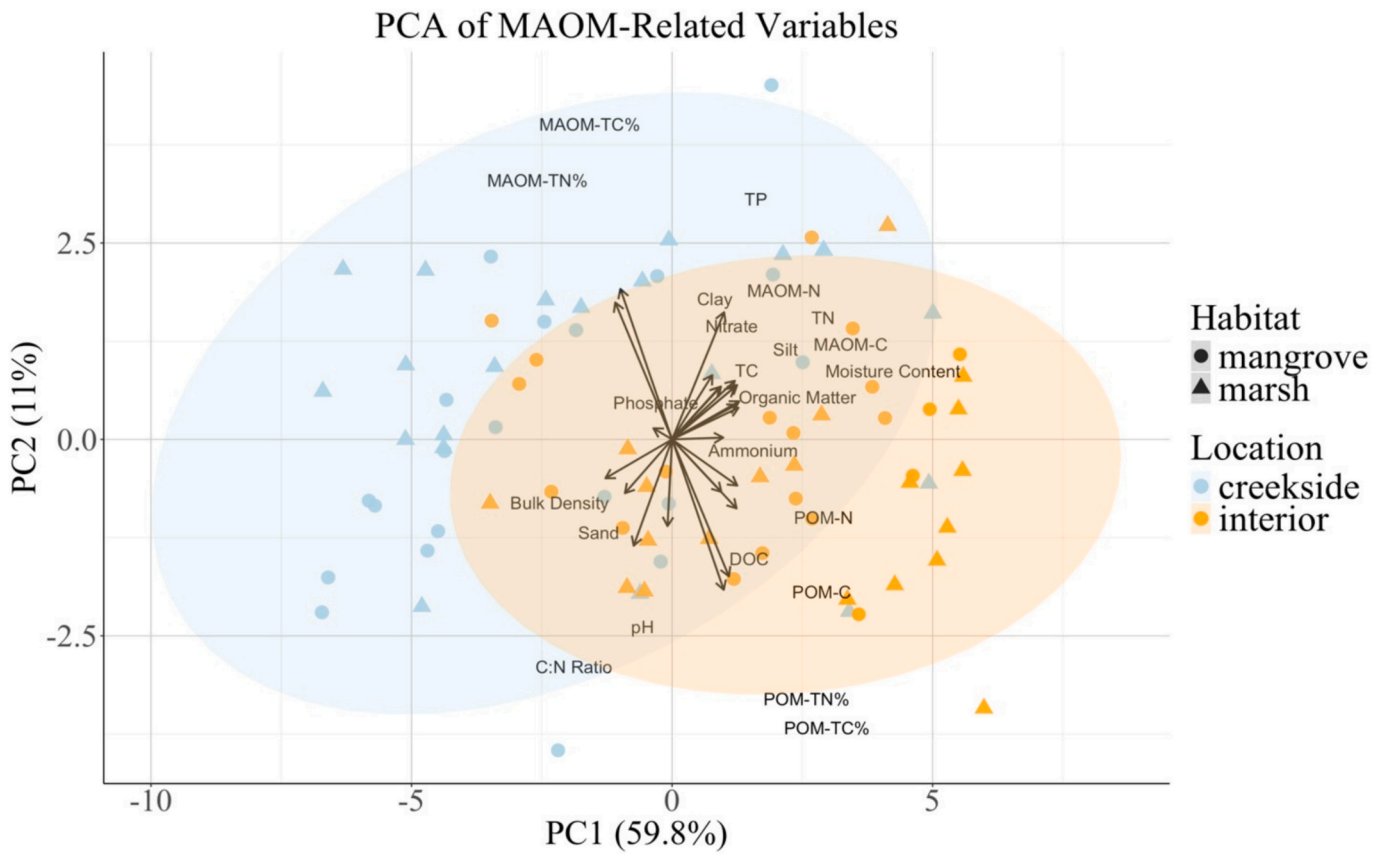

Fig. 6. Principal component analysis (PCA) of soil physicochemical and MAOM-related variables across marsh and mangrove plots. Points represent individual soil samples colored by location (creekside vs. interior) and shaped by vegetation (marsh vs. mangrove), with ellipses indicating 95% confidence intervals based on location (creekside vs. interior). Arrows represent the direction and relative contribution of each variable to the first two principal component.

4.2. Mangrove and marsh responses to nitrogen enrichment in the interior

Results suggest that N addition increased MAOM-C and MAOM-N in interior mangrove plots but reduced these pools in interior marsh plots (Fig. 3A;3B). No notable increase in *A. germinans* stem height or root productivity was documented in fertilized interior mangrove plots (Bravo et al., in review). The impact of nutrient addition on mangrove productivity in other studies has been mixed. While N enrichment generally promotes aboveground growth and productivity in mangroves (Dangremond et al., 2020; Mack et al., 2024), its effects on belowground allocation are variable. Some studies report decreased mangrove root-to-shoot ratios under fertilization (Lovelock et al., 2009; Hayes et al., 2017), whereas others observe increases in root biomass (Weaver and Armitage, 2020).

Since no effect of fertilization on mangrove productivity was observed in this study, the mechanism for enhanced MAOM formation in these plots may be more nuanced. Mangroves are known to reallocate nutrients belowground prior to senescence (Reef et al., 2010), have greater root exudation of C (Komiyama et al., 2008), and demonstrate niche differentiation in nutrient uptake when competing with marsh grasses (Dangremond et al., 2020), all of which could contribute to increased microbial processing and MAOM formation. Moreover, NH_4^+, the preferred N form for mangrove uptake (Alongi et al., 1994; Reef et al., 2010), was higher in fertilized mangrove plots (Fig. 5B), potentially supporting greater microbial processing efficiency and the *in vivo* MAOM formation. According to the *in vivo* MAOM formation theory, microbes assimilate organic substrates and their necromass becomes stabilized post-mortem via mineral binding (Cotrufo and Lavallee, 2022). Mangrove roots may also enhance MAOM by delivering fresh C deeper into the soil than marsh roots, increasing the likelihood of interactions with reactive mineral surfaces (Sokol et al., 2019). Finally, mangrove roots can oxygenate surrounding sediments and create steep redox gradients, which stimulate the formation of reactive Fe oxides capable of binding OM (Kristensen et al., 2008; Adhikari et al., 2017; Dicen et al., 2019). Overall, fertilized mangroves may enhance MAOM formation with elevated NH_4^+ availability, accelerated root turnover, rhizosphere redox processes, and enhanced microbial processing, but additional mechanistic studies are needed and the response may be site-specific.

In contrast, MAOM-C and MAOM-N decreased in fertilized interior marsh plots (Fig. 3A, B). Because root productivity and stem density of *S. alterniflora* did not increase with fertilization (Bravo et al., in review), this species (being a C_4 grass) may have lower nutrient responsiveness or lower belowground allocation under high N. While N addition can stimulate growth in salt marshes, the lower nutrient demand of C_4 species may limit nutrient uptake and belowground C inputs (Sterner and Elser, 2002). Other work has demonstrated that chronic nutrient enrichment in *S. alterniflora* marshes can reduce belowground biomass by over 50%, increase decomposition rates, and lead to net SOM loss (Turner et al., 2009; Deegan et al., 2012). Though some wetlands show increased rhizome production and belowground productivity under moderate N enrichment (Morris and Sundberg, 2024) indicating, responses remain highly context-dependent. In this study, elevated DOC concentrations in fertilized marsh plots (Fig. 5A) suggests the added N was stimulating soil decomposition and C loss through tidal export or leaching (Wang et al., 2014) resulting in a lower microbial stabilization efficiency (Zhang et al., 2025). These findings indicate that despite the lability of *S. alterniflora* litter, high nutrient loads may reduce C use efficiency or alter microbial communities, limiting MAOM formation because more C is retained in the dissolved phase or exported from the

system. Additionally, nutrient enrichment may disadvantage marsh grasses in competitive settings. Previous work shows that *S. alterniflora* cover declines in fertilized mangrove plots, likely due to rapid overtopping by *A. germinans* under high N availability (Dangremond et al., 2020). Data from our plots indicates *A. germinans* seedlings and *Batis maritima* significantly increased in stem height in fertilized interior marsh plots where *S. alterniflora* did not (Bravo et al., in review).

Despite reduced MAOM in fertilized marshes, these ecosystems may still contribute to stabilization via *ex vivo* pathways, where microbial enzymes break down plant litter into soluble compounds that bind to minerals (Cotrufo and Lavallee, 2022). Under low nutrient conditions, marshes may even hold an advantage: our results showed that control marsh plots outperformed control mangroves in MAOM-C and MAOM-N, likely due to simpler litter chemistry and more efficient microbial transformation consistent with the MEMS framework (Cotrufo et al., 2013). These patterns highlight the sensitivity of SOM stabilization to both nutrient inputs and plant traits.

Notably, fertilized marshes retained more C in POM than MAOM, while mangroves showed the reverse, suggesting marshes rely more on detrital accumulation, whereas mangroves favor microbial processing pathways. In addition to plant litter quality and hydrologic context, microbial community structure, particularly fungal–bacterial balance, may contribute to the contrasting SOM partitioning observed in fertilized marshes. While POM is commonly conceptualized as a detrital plant-derived pool, its formation and persistence can be indirectly shaped by fungal activity through aggregation and residue processing (Six et al., 2006; Cotrufo et al., 2013; Kim et al., 2022). Higher fungal-to-bacterial ratios have been associated with greater POM retention through slower SOM mineralization (Craig et al., 2018; Malik et al., 2016). POM-N was also more variable across marsh plots, potentially reflecting rapid turnover or loss, whereas MAOM-N responses in mangroves were more consistent. The tendency for fertilized mangroves to store a larger proportion of organic inputs in MAOM (by mass and percent of the TC and TN pools) emphasizes the role of mangroves in long-term C and N stabilization.

4.3. Mangrove and marsh responses to nitrogen enrichment in the creekside

In creekside, fertilized marsh plots contained more MAOM-C and MAOM-N than fertilized mangroves (Fig. 3A;3B), the opposite to interior plot trends. Root productivity also tended to be lower in creekside mangrove plots compared to interior mangroves (Bravo et al., in review), suggesting that hydrodynamic stressors (such as frequent tidal flushing, sediment instability, and elevated salinity) could override the effect of nutrient availability and plant traits (Langley et al., 2013; Domínguez-Cadena et al., 2016). Moreover, in the dynamic creekside zones more frequent tidal flushing may enhance nutrient availability, reducing the need for extensive mangrove root systems. However, physical stressors such as sediment instability and rapid porewater turnover may still limit belowground C allocation and microbial stabilization pathways, ultimately constraining MAOM formation in mangroves despite fertilization.

In contrast, *S. alterniflora* is well-adapted to salinity and tidal stress (Mendelssohn et al., 2000). Its dominance at creek edges, likely aided by reduced competition, may promote SOM accumulation despite harsh conditions and explain the larger MAOM and POM pools in fertilized marshes. Interestingly, no differences were observed between control marsh and mangrove plots, indicating that nutrient addition, not vegetation alone, drives divergence under stress. Moreover, while mass differences in MAOM-C and POM-C concentrations existed between vegetation types, no difference was observed when normalized to soil TC. These findings underscore how spatial context mediates SOM stabilization responses to nutrient inputs. In dynamic creekside environments, abiotic filtering can dampen fertilization responses in mangroves, while marsh vegetation may retain greater C under similar conditions. Additionally, nutrient enrichment effects were weaker in creekside zones than in interior zones, indicating that hydrologic forcing and sediment dynamics can override treatment impacts on OM stabilization.

4.4. Implications for carbon sequestration in changing coastal ecosystems

Understanding how N enrichment affects soil C stabilization at a marsh-mangrove ecotone is essential for guiding C sequestration strategies and predicting long-term soil C pools during ecosystem change. While prior studies have emphasized changes in vegetation, aboveground biomass, and total SOC (Doughty et al., 2016; Dangremond et al., 2020), fewer have focused on impacts to MAOM and POM fractions— the functionally and structurally distinct pools with different stabilization mechanisms (Lavallee et al., 2020; Cotrufo and Lavallee, 2022). Our findings suggest that mangrove presence, when combined with N inputs, promotes MAOM formation in interior zones where reduced flushing, fine sediments, and elevated organic inputs create favorable stabilization conditions. This aligns with prior work documenting enhanced SOC burial in northern Florida's mangrove–marsh ecotones (Doughty et al., 2016; Vaughn et al., 2020, 2021). Mangroves may facilitate stabilization via both productivity (Komiyama et al., 2008) and high-quality microbial inputs via root exudates and turnover (Sokol et al., 2019). However, this experiment does not address progressive mangrove encroachment over time or how SOM dynamics evolve during mangrove invasion.

Our results show that vegetation responses to N fertilization are strongly context-dependent: while interior mangroves tended to enhance MAOM under N addition, fertilized mangroves in creekside locations formed less MAOM than marshes, likely due to hydrodynamic stressors that reduce microbial efficiency and C inputs (Mangora, 2016; Alongi, 2020). These zonal differences highlight the importance of hydrogeomorphic context in shaping C sequestration potential (Fagherazzi and Mariotti, 2012). While several studies document greater aboveground biomass when mangroves replace marsh vegetation, our findings suggest that the impact on belowground SOM stabilization processes is nonuniform. This is consistent with Steinmuller et al. (2022), who found that soil OC density is more influenced by environmental setting and time since encroachment than by dominant vegetation alone. Therefore, site-specific and hydrogeomorphic-specific assessments of SOM dynamics are essential for accurately evaluating C sequestration outcomes and informing restoration planning.

Finally, coastal wetlands may exhibit a trade-off between the size of SOM pools and their stabilization efficiency—a pattern that warrants deeper investigation across other estuarine systems (Assavapanuvat et al., 2024; Zhang et al., 2024). By quantifying C in both MAOM and POM pools, our study advances a mechanistic understanding of how vegetation, soil, and hydrology interact to shape C fate. Future research should expand these approaches to broader spatial scales and include isotopic tracing, microbial community profiling, and longer-term monitoring to better predict how C storage responds to climate and nutrient pressures across diverse coastal settings.

5. Conclusion

This study aimed to determine how N enrichment and differences in marsh and mangrove vegetation influence the stability of SOM—particularly the formation of MAOM— across distinct hydrogeomorphic settings. Our results show that SOM stabilization responses are strongly shaped by environmental context, producing divergent outcomes for C preservation depending on landscape position relative to tidal creeks. Specifically, interior wetlands accumulated greater quantities of SOM and MAOM, reflecting reduced tidal exchange, finer sediments, and greater OM retention. Meanwhile, creekside wetlands had lower overall SOM accumulation but a higher proportion of MAOM. This pattern highlights a fundamental trade-off between OM accumulation

and stabilization efficiency, which differs across hydrogeomorphic positions. Vegetation type further modified these patterns, as mangrove soils promoted greater MAOM formation under N enrichment in low-energy interior settings, whereas marsh soils showed reduced MAOM under similar conditions; differences in plant traits, nutrient demand, and belowground processing pathways likely explain this divergent response and merit further investigation. In creekside environments, physical stressors appeared to constrain mangrove contributions to SOM stabilization, while marsh vegetation maintained or enhanced OM retention.

Together, this study underscores that predictions of C sequestration outcomes based solely on vegetation shifts or nutrient loading may be misleading without explicit consideration of landscape context. As mangroves continue to expand poleward and nutrient enrichment intensifies in coastal regions, site-specific approaches that explicitly incorporate hydrogeomorphic context are needed. Incorporating this complexity will improve the accuracy of long-term C storage projections and aid in the design of effective restoration and climate mitigation strategies in coastal wetlands.

CRediT authorship contribution statement

Mercedes M. Pinzon: Visualization, Methodology, Investigation, Formal analysis, Conceptualization, Writing – review & editing, Writing – original draft. **Jocelyn Bravo:** Writing – review & editing. **Samantha K. Chapman:** Supervision, Funding acquisition, Writing – review & editing. **J. Adam Langley:** Project administration, Funding acquisition, Writing – review & editing. **Lisa G. Chambers:** Supervision, Resources, Project administration, Funding acquisition, Data curation, Conceptualization, Writing – review & editing.

Declaration of competing interest

We have nothing to declare.

Acknowledgments

This research was conducted as part of the WETFEET project funded by the National Science Foundation, Division of Environmental Biology, Collaborative Grant Award #2224999 and #2225000 to Villanova University and the University of Central Florida, and the Department of Biology at the University of Central Florida. The authors would like to thank Nikki Dix, members of the Aquatic Biogeochemistry Lab (ABL; Naija Cheek, Jennifer Volk, Anthony Mirabito, and Anastasiia Pestereva) for their support and assistance throughout this project with filed sample collection and laboratory analysis, as well as to the collaborators at Villanova University (Tess Adgie and Cathilyn McIntosh) for their support and assistance with field experiment design and data analysis. The authors also thank Drs. Linda Walters, and Christian Fleming for numerous discussions that informed this research.

Appendix A. Supplementary data

Supplementary data to this article can be found online at https://doi.org/10.1016/j.scitotenv.2026.181643.

Data availability

Data will be made available on request.

References

Adhikari, D., Zhao, Q., Das, K., Mejia, J., Huang, R., Wang, X., Poulson, S.R., Tang, Y., Roden, E.E., Yang, Y., 2017. Dynamics of ferrihydrite-bound organic carbon during microbial Fe reduction. Geochim. Cosmochim. Acta 212, 221–233. https://doi.org/10.1016/j.gca.2017.06.017.

Allen, A.C., Beck, C.A., Sattelberger, D.C., Kiszka, J.J., 2022. Evidence of a dietary shift by the Florida manatee (Trichechus manatus latirostris) in the Indian River Lagoon inferred from stomach content analyses. Estuar. Coast. Shelf Sci. 268, 107788. https://doi.org/10.1016/j.ecss.2022.107788.

Alongi, D.M., 2014. Carbon cycling and storage in mangrove forests. Annu. Rev. Mar. Sci. 6 (1), 195–219. https://doi.org/10.1146/annurev-marine-010213-135020.

Alongi, D.M., 2020. Nitrogen cycling and mass balance in the world's mangrove forests. Nitrogen 1 (2), 167–189. https://doi.org/10.3390/nitrogen1020014.

Alongi, D.M., Marshall, N., Macintosh, D., Sasekumar, A., 1994. The role of bacteria in nutrient recycling in tropical mangrove and other coastal benthic ecosystems. Hydrobiologia 285 (1–3), 19–32. https://doi.org/10.1007/bf00005650.

Andersen, J., 1976. An ignition method for determination of total phosphorus in lake sediments. Water Res. 10 (4), 329–331. https://doi.org/10.1016/0043-1354(76)90175-5.

Assavapanuvat, P., Breithaupt, J.L., Engelbert, K.M., Schröder, C., Smoak, J.M., Bianchi, T.S., 2024. Contrasting stocks and origins of particulate and mineral-associated soil organic carbon in a mangrove-salt marsh ecotone. Geoderma 446, 116904. https://doi.org/10.1016/j.geoderma.2024.116904.

Barreto, C.R., Morrissey, E.M., Wykoff, D.D., Chapman, S.K., 2018. Co-occurring mangroves and salt marshes differ in microbial community composition. Wetlands 38 (3), 497–508. https://doi.org/10.1007/s13157-018-0994-9.

Barton, K., 2023. MuMIn: Multi-Model Inference. R package version 1.47.1. https://cran.rproject.org/package=MuMIn.

Bianchi, T.S., Allison, M.A., Zhao, J., Li, X., Comeaux, R.S., Feagin, R.A., Kulawardhana, R.W., 2013. Historical reconstruction of mangrove expansion in the Gulf of Mexico: linking climate change with carbon sequestration in coastal wetlands. Estuar. Coast. Shelf Sci. 119, 7–16. https://doi.org/10.1016/j.ecss.2012.12.007.

Bouillon, S., Borges, A.V., Castañeda-Moya, E., Diele, K., Dittmar, T., Duke, N.C., Kristensen, E., Lee, S.Y., Marchand, C., Middelburg, J.J., Rivera-Monroy, V.H., Smith, T.J., Twilley, R.R., 2008. Mangrove production and carbon sinks: a revision of global budget estimates. Glob. Biogeochem. Cycles 22 (2), 2013. https://doi.org/10.1029/2007GB003052.

Breithaupt, J.L., Smoak, J.M., Sanders, C.J., Troxler, T.G., 2019. Spatial variability of organic carbon, CaCO3 and nutrient burial rates spanning a mangrove productivity gradient in the coastal everglades. Ecosystems 22 (4), 844–858. https://doi.org/10.1007/s10021-018-0306-5.

Bricker, S.B., Longstaff, B., Dennison, W., Jones, A., Boicourt, K., Wicks, C., Woerner, J., 2008. Effects of nutrient enrichment in the nation's estuaries: a decade of change. Harmful Algae 8 (1), 21–32. https://doi.org/10.1016/j.hal.2008.08.028.

Cahoon, D.R., McKee, K.L., Morris, J.T., 2021. How plants influence resilience of salt marsh and mangrove wetlands to sea-level rise. Estuar. Coasts 44 (4), 883–898. https://doi.org/10.1007/s12237-020-00834-w.

Cambardella, C.A., Elliott, E.T., 1992. Particulate soil organic-matter changes across a grassland cultivation sequence. Soil Sci. Soc. Am. J. 56 (3), 777–783. https://doi.org/10.2136/sssaj1992.03615995005600030017x.

Castellano, M.J., Mueller, K.E., Olk, D.C., Sawyer, J.E., Six, J., 2015. Integrating plant litter quality, soil organic matter stabilization, and the carbon saturation concept. Glob. Chang. Biol. 21 (9), 3200–3209. https://doi.org/10.1111/gcb.12982.

Cavanaugh, K.C., Kellner, J.R., Forde, A.J., Gruner, D.S., Parker, J.D., Rodriguez, W., Feller, I.C., 2014. The poleward expansion of mangroves is a threshold response to the decreased frequency of extreme cold events. Proc. Natl. Acad. Sci. 111 (2), 723–727. https://doi.org/10.1073/pnas.1315800111.

Cavanaugh, K.C., Dangremond, E.M., Doughty, C.L., Williams, A.P., Parker, J.D., Hayes, M.A., Rodriguez, W., Feller, I.C., 2019. Climate-driven regime shifts in a mangrove–salt marsh ecotone over the past 250 years. Proc. Natl. Acad. Sci. 116 (43), 21602–21608. https://doi.org/10.1073/pnas.1902181116.

CENR, 2000. Integrated Assessment of Hypoxia in the Northern Gulf of Mexico. National Science and Technology Council Committee on Environment and Natural Resources.

Chambers, L.G., Steinmuller, H.E., Breithaupt, J.L., 2019. Toward a mechanistic understanding of "peat collapse" and its potential contribution to coastal wetland loss. Ecology 100 (7), 1–15. https://doi.org/10.1002/ecy.2720. Durham.

Chapman, S.K., Feller, I.C., Canas, G., Hayes, M., Dix, N., Hester, M., Morris, J., Langley, J.A., 2021. Mangrove growth response to experimental warming is greatest near the range limit in northeast Florida. Ecology 102 (6), 1–11. https://doi.org/10.1002/ecy.3320. Durham.

Chmura, G.L., Anisfeld, S.C., Cahoon, D.R., Lynch, J.C., 2003. Global carbon sequestration in tidal, saline wetland soils. Glob. Biogeochem. Cycles 17 (4), 2002GB001917. https://doi.org/10.1029/2002GB001917.

Cloern, J.E., 2001. Our evolving conceptual model of the coastal eutrophication problem. Mar. Ecol. Prog. Ser. 210, 223–253. https://doi.org/10.3354/meps210223.

Coldren, G.A., Langley, J.A., Feller, I.C., Chapman, S.K., 2019. Warming accelerates mangrove expansion and surface elevation gain in a subtropical wetland. J. Ecol. 107 (1), 79–90. https://doi.org/10.1111/1365-2745.13049.

Cooray, I.G., Chalmers, G., Chittleborough, D., 2025. A review of properties of organic matter fractions in soils of mangrove wetlands: Implications for carbon storage. Soil Biol. Biochem. 201, 109660. https://doi.org/10.1016/j.soilbio.2024.109660.

Cotrufo, M.F., Lavallee, J.M., 2022. Soil organic matter formation, persistence, and functioning: a synthesis of current understanding to inform its conservation and regeneration. In: Sparks, D.L. (Ed.), Advances in Agronomy. Academic Press, pp. 1–66. https://doi.org/10.1016/bs.agron.2021.11.002.

Cotrufo, M.F., Wallenstein, M.D., Boot, C.M., Denef, K., Paul, E., 2013. The microbial efficiency-matrix stabilization (MEMS) framework integrates plant litter decomposition with soil organic matter stabilization: do labile plant inputs form stable soil organic matter? Glob. Chang. Biol. 19 (4), 988–995. https://doi.org/10.1111/gcb.12113.

Cotrufo, M.F., Soong, J.L., Horton, A.J., Campbell, E.E., Haddix, M.L., Wall, D.H., Parton, W.J., 2015. Formation of soil organic matter via biochemical and physical pathways of litter mass loss. Nat. Geosci. 8 (10), 776–779. https://doi.org/10.1038/ngeo2520.

Craig, M.E., Turner, B.L., Liang, C., Clay, K., Johnson, D.J., Phillips, R.P., 2018. Tree mycorrhizal type predicts within-site variability in the storage and distribution of soil organic matter. Glob. Chang. Biol. 24 (8), 3317–3330. https://doi.org/10.1111/gcb.14132.

Dangremond, E.M., Simpson, L.T., Osborne, T.Z., Feller, I.C., 2020. Nitrogen enrichment accelerates mangrove range expansion in the temperate–tropical ecotone. Ecosyst 23 (4), 703–714. https://doi.org/10.1007/s10021-019-00441-2.

Deegan, L.A., Bowen, J.L., Drake, D., Fleeger, J.W., Friedrichs, C.T., Galván, K.A., Hobbie, J.E., Hopkinson, C., Johnson, D.S., Johnson, J.M., LeMay, L.E., Miller, E., Peterson, B.J., Picard, C., Sheldon, S., Sutherland, M., Vallino, J., Warren, R.S., 2007. Susceptibility of salt marshes to nutrient enrichment and predator removal. Ecol. Appl. 17 (5), 42–63. https://doi.org/10.1890/06-0452.1.

Deegan, L.A., Johnson, D.S., Warren, R.S., Peterson, B.J., Fleeger, J.W., Fagherazzi, S., Wollheim, W.M., 2012. Coastal eutrophication as a driver of salt marsh loss. Nature 490 (7420), 388–392. https://doi.org/10.1038/nature11533.

Dicen, G.P., Navarrete, I.A., Rallos, R.V., Salmo, S.G., Garcia, M.C.A., 2019. The role of reactive iron in long-term carbon sequestration in mangrove sediments. J. Soils Sediments 19 (1), 501–510. https://doi.org/10.1007/s11368-018-2051-y.

Domínguez-Cadena, R., Riosmena-Rodríguez, R., Luz, J.L.L., 2016. Forest structure and species composition of mangroves in the eastern Baja California peninsula: the role of microtopography. Wetlands 36 (3), 515–523. https://doi.org/10.1007/s13157-016-0760-9.

Doughty, C.L., Langley, J.A., Walker, W.S., Feller, I.C., Schaub, R., Chapman, S.K., 2016. Mangrove range expansion rapidly increases coastal wetland carbon storage. Estuar. Coasts 39 (2), 385–396. https://doi.org/10.1007/s12237-015-9993-8.

Duarte, C.M., Thampanya, U., Terrados, J., Geertz-Hansen, O., tes, M., 1999. The determination of the age and growth of SE Asian mangrove seedlings from internodal counts. Mangrove Salt Marshes 3 (4), 251–257. https://doi.org/10.1023/A:1009967401337.

Fagherazzi, S., Mariotti, G., 2012. Mudflat runnels: evidence and importance of very shallow flows in intertidal morphodynamics. Geophys. Res. Lett. 39 (14). https://doi.org/10.1029/2012GL052542.

Feller, I.C., Whigham, D.F., McKee, K.L., Lovelock, C.E., 2003. Nitrogen limitation of growth and nutrient dynamics in a disturbed mangrove forest, Indian River lagoon, Florida. Oecologia 134 (3), 405–414. https://doi.org/10.1007/s00442-002-1117-z.

Feller, I.C., Lovelock, C.E., McKee, K.L., 2007. Nutrient addition differentially affects ecological processes of *Avicennia germinans* in nitrogen versus phosphorus limited mangrove ecosystems. Ecosystems 10 (3), 347–359. https://doi.org/10.1007/s10021-007-9025-z. New York.

Galloway, J.N., Townsend, A.R., Erisman, J.W., Bekunda, M., Cai, Z., Freney, J.R., Martinelli, L.A., Seitzinger, S.P., Sutton, M.A., 2008. Transformation of the nitrogen cycle: recent trends, questions, and potential solutions. Science 320 (5878), 889–892. https://doi.org/10.1126/science.1136674.

Graham, S.A., Mendelssohn, I.A., 2014. Coastal wetland stability maintained through counterbalancing accretionary responses to chronic nutrient enrichment. Ecology 95 (12), 3271–3283. https://doi.org/10.1890/14-0196.1. Durham.

Hamada, K., Ohtsuka, T., Fujitake, N., Miyajima, T., Yokoyama, Y., Miyairi, Y., Kida, M., 2024. Functional organic matter components in mangrove soils revealed by density fractionation. Soil Sci. Plant Nutr. 70 (2), 88–99. https://doi.org/10.1080/00380768.2024.2304761.

Hartig, F., Lohse, L., 2022. DHARMa: residual diagnostics for hierarchical (multi-level / mixed) regression models. R package version 0.4.5. https://cran.r-project.org/package=DHARMa.

Hayes, M.A., Jesse, A., Tabet, B., Reef, R., Keuskamp, J.A., Lovelock, C.E., 2017. The contrasting effects of nutrient enrichment on growth, biomass allocation and decomposition of plant tissue in coastal wetlands. Plant Soil 416 (1/2), 193–204. https://doi.org/10.1007/s11104-017-3206-0.

Hupp, C.R., Pierce, A.R., Noe, G.B., 2009. Floodplain geomorphic processes and environmental impacts of human alteration along Coastal Plain rivers, USA. Wetlands 29 (2), 413–429. https://doi.org/10.1672/08-169.1.

Hurst, N., White, J.R., Baustian, J., 2016. Nitrate reduction in a hydrologically restored bottomland hardwood Forest in the Mississippi River Watershed, Northern Louisiana. Soil Sci. Soc. Am. J. 80 (6), 1698–1705. https://doi.org/10.2136/sssaj2016.08.0250.

Kelleway, J.J., Saintilan, N., Macreadie, P.I., Skilbeck, C.G., Zawadzki, A., Ralph, P.J., 2016. Seventy years of continuous encroachment substantially increases 'blue carbon' capacity as mangroves replace intertidal salt marshes. Glob. Chang. Biol. 22 (3), 1097–1109. https://doi.org/10.1111/gcb.13158.

Kelleway, J.J., Cavanaugh, K., Rogers, K., Feller, I.C., Ens, E., Doughty, C., Saintilan, N., 2017. Review of the ecosystem service implications of mangrove encroachment into salt marshes. Glob. Chang. Biol. 23 (10), 3967–3983. https://doi.org/10.1111/gcb.13727.

Kim, K., Neuberger, P., Daly, E.J., Gorzelak, M., Hernandez-Ramirez, G., 2022. Arbuscular mycorrhizal fungi community linkages to soil nutrient availability across contrasting agroecosystems. Appl. Soil Ecol. A Section Agric. Ecosyst. Environ. 176, 104464. https://doi.org/10.1016/j.apsoil.2022.104464.

Kleber, M., 2010. What is recalcitrant soil organic matter? Environ. Chem. 7 (4), 320–332. https://doi.org/10.1071/EN10006.

Kleber, M., Eusterhues, K., Keiluweit, M., Mikutta, C., Mikutta, R., Nico, P.S., 2015. Mineral–organic associations: formation, properties, and relevance in soil environments. In: Advances in Agronomy, 130. Elsevier, pp. 1–140. https://doi.org/10.1016/bs.agron.2014.10.005.

Komiyama, A., Ong, J.E., Poungparn, S., 2008. Allometry, biomass, and productivity of mangrove forests: a review. Aquat. Bot. 89 (2), 128–137. https://doi.org/10.1016/j.aquabot.2007.12.006.

Krauss, K.W., Doyle, T.W., Twilley, R.R., Smith, T.J., Whelan, K.R.T., Sullivan, J.K., 2011. Sea-level rise and landscape change influence mangrove encroachment onto marsh in the Ten Thousand Islands region of Florida. *USA*. J. Coast. Conserv. 15 (4), 629–638. https://doi.org/10.1007/s11852-011-0153-4.

Krauss, K.W., McKee, K.L., Lovelock, C.E., Cahoon, D.R., Saintilan, N., Reef, R., Chen, L., 2014. How mangrove forests adjust to rising sea level. New Phytol. 202 (1), 19–34. https://doi.org/10.1111/nph.12605.

Kristensen, E., Bouillon, S., Dittmar, T., Marchand, C., 2008. Organic carbon dynamics in mangrove ecosystems: a review. Aquat. Bot. 89 (2), 201–219. https://doi.org/10.1016/j.aquabot.2007.12.005.

Langley, J.A., Mozdzer, T.J., Shepard, K.A., Hagerty, S.B., Megonigal, J.P., 2013. Tidal marsh plant responses to elevated CO2, nitrogen fertilization, and sea level rise. Glob. Chang. Biol. 19 (5), 1495–1503. https://doi.org/10.1111/gcb.12147.

Lapointe, B.E., Herren, L.W., Debortoli, D.D., Vogel, M.A., 2015. Evidence of sewage driven eutrophication and harmful algal blooms in Florida's Indian River lagoon. Harmful Algae 43, 82–102. https://doi.org/10.1016/j.hal.2015.01.004.

Lapointe, B.E., Herren, L.W., Brewton, R.A., Alderman, P.K., 2020. Nutrient over enrichment and light limitation of seagrass communities in the Indian River lagoon, an urbanized subtropical estuary. Sci. Total Environ. 699, 134068. https://doi.org/10.1016/j.scitotenv.2019.134068.

Lavallee, Jocelyn M., Soong, J.L., Cotrufo, M.F., 2020. Conceptualizing soil organic matter into particulate and mineral-associated forms to address global change in the 21st century. Glob. Chang. Biol. 26 (1), 261–273. https://doi.org/10.1111/gcb.14859.

Lê, S., Josse, J., Husson, F., 2008. FactoMineR: an R package for multivariate analysis. J. Stat. Softw. 25 (1), 1–18. https://doi.org/10.18637/jss.v025.i01.

Lehmann, J., Kleber, M., 2015. The contentious nature of soil organic matter. Nature (London) 528 (7580), 60–68. https://doi.org/10.1038/nature16069.

Lenth, R., 2020. Emmeans: estimated marginal means, aka least-squares means (R package version 1.5.2-1). https://CRAN.R-project.org/package=emmeans.

Lewis, D.B., Jimenez, K.L., Abd-Elrahman, A., Andreu, M.G., Landry, S.M., Northrop, R. J., Campbell, C., Flower, H., Rains, M.C., Richards, C.L., 2021. Carbon and nitrogen pools and mobile fractions in surface soils across a mangrove saltmarsh ecotone. Sci. Total Environ. 798, 149328. https://doi.org/10.1016/j.scitotenv.2021.149328.

Lovelock, C.E., Ball, M.C., Martin, K.C., Feller, C., 2009. Nutrient enrichment increases mortality of mangroves. PLoS One 4 (5), 5600. https://doi.org/10.1371/journal.pone.0005600.

Lüdecke, D., Ben-Shachar, M., Patil, I., Waggoner, P., Makowski, D., 2021. Performance: an R package for assessment, comparison and testing of statistical models. J. Open Source Software 6 (60), 3139. https://doi.org/10.21105/joss.03139.

Mack, M.R., Langley, J.A., Feller, I.C., Chapman, S.K., 2024. The ecological consequences of nutrient enrichment in mangroves. Estuar. Coast. Shelf Sci. 300, 108690. https://doi.org/10.1016/j.ecss.2024.108690.

Malik, A.A., Chowdhury, S., Schlager, V., Oliver, A., Puissant, J., Vazquez, P.G.M., Jehmlich, N., Bergen, M., Griffiths, R.I., Gleixner, G., 2016. Soil fungal: bacterial ratios are linked to altered carbon cycling. Front. Microbiol. 7, 1247. https://doi.org/10.3389/fmicb.2016.01247.

Mangora, M.M., 2016. Nutrient enrichment and saline conditions decreases growth and photosynthesis of the mangrove Heritiera littoralis Dryand. Open J. Marine Sci. 6 (2), 293–301. https://doi.org/10.4236/ojms.2016.62024.

Mazerolle, M.J., 2020. *AICcmodavg: Model selection and multimodel inference based on (Q) AIC(c) (Version 2.3-4) [R package]* [Computer software]. Comprehensive R Archive Network. https://cran.r-project.org/package=AICcmodavg.

McKee, K.L., Cahoon, D.R., Feller, I.C., 2007. Caribbean mangroves adjust to rising sea level through biotic controls on change in soil elevation. Glob. Ecol. Biogeogr. 16 (5), 545–556. https://doi.org/10.1111/j.1466-8238.2007.00317.x.

Mendelssohn, I.A., Morris, J.T., Kreeger, D.A., Weinstein, M.P., 2000. Eco-physiological controls on the productivity of *Spartina Alterniflora* Loisel. In: Concepts and Controversies in Tidal Marsh Ecology. Springer Netherlands, pp. 59–80. https://doi.org/10.1007/0-306-47534-0_5.

Millard, S.P., Kowarik, A., 2025. *EnvStats: An R Package for Environmental Statistics, including US EPA guidance (Version 3.1.0) [R package]* [Computer software]. Comprehensive R Archive Network. https://cran.r-project.org/package=EnvStats.

Mirabito, A.J., Chambers, L.G., 2023. Quantifying mineral-associated organic matter in wetlands as an indicator of the degree of soil carbon protection. Geoderma 430, 116327. https://doi.org/10.1016/j.geoderma.2023.116327.

Morris, J.T., Sundberg, K., 2024. Responses of coastal wetlands to rising sea-level revisited: the importance of organic production. Estuar. Coasts 47 (7), 1735–1749. https://doi.org/10.1007/s12237-023-01313-8.

Morris, J., Sundberg, K., Hopkinson, C., 2013. Salt marsh primary production and its responses to relative sea level and nutrients in estuaries at Plum Island, Massachusetts, and North Inlet, South Carolina, USA. Oceanography 26 (3), 78–84. https://doi.org/10.5670/oceanog.2013.48.

N.O.A.A., 2024. National Climate Data Center website. Retrieved. https://www.ncdc.noaa.gov/cdo-web/webservices.

Ofiti, N.O.E., Schmidt, M.W.I., Abiven, S., Hanson, P.J., Iversen, C.M., Wilson, R.M., Kostka, J.E., Wiesenberg, G.L.B., Malhotra, A., 2023. Climate warming and elevated CO2 alter peatland soil carbon sources and stability. Nat. Commun. 14 (1), 7533. https://doi.org/10.1038/s41467-023-43410-z.

Osland, M.J., Enwright, N., Day, R.H., Doyle, T.W., 2013. Winter climate change and coastal wetland foundation species: salt marshes vs. mangrove forests in the southeastern United States. Glob. Chang. Biol. 19 (5), 1482–1494. https://doi.org/10.1111/gcb.12126.

Osland, M.J., Stevens, P.W., Lamont, M.M., Brusca, R.C., Hart, K.M., Waddle, J.H., Langtimm, C.A., Williams, C.M., Keim, B.D., Terando, A.J., Reyier, E.A., Marshall, K. E., Loik, M.E., Boucek, R.E., Lewis, A.B., Seminoff, J.A., 2021. Tropicalization of temperate ecosystems in North America: the northward range expansion of tropical organisms in response to warming winter temperatures. Glob. Chang. Biol. 27 (13), 3009–3034. https://doi.org/10.1111/gcb.15563.

Overstreet, K., Dangremond, E.M., Feller, I.C., 2025. Frozen green leaves as potential nutrient subsidies in North American mangrove ecosystems. Estuar. Coasts 48 (2), 30. https://doi.org/10.1007/s12237-024-01457-1.

Peterson, P.M., Romaschenko, K., Arrieta, Y.H., Saarela, J.M., 2014. A molecular phylogeny and new subgeneric classification of *Sporobolus* (Poaceae: Chloridoideae: Sporobolinae). TAXON 63 (6), 1212–1243. https://doi.org/10.12705/636.19.

Reddy, K.R., DeLaune, R.D., 2008. Biogeochemistry of Wetlands, 0 ed. CRC Press. https://doi.org/10.1201/9780203491454.

Reddy, K.R., Patrick, W.H., 1975. Effect of alternate aerobic and anaerobic conditions on redox potential, organic matter decomposition and nitrogen loss in a flooded soil. Soil Biol. Biochem. 7 (2), 87–94. https://doi.org/10.1016/0038-0717(75)90004-8.

Reef, R., Feller, I.C., Lovelock, C.E., 2010. Nutrition of mangroves. Tree Physiol. 30 (9), 1148–1160. https://doi.org/10.1093/treephys/tpq048.

Rodriguez, W., Feller, I.C., Cavanaugh, K.C., 2016. Spatio-temporal changes of a mangrove–saltmarsh ecotone in the northeastern coast of Florida, USA. Global Ecol. Conserv. 7, 245–261. https://doi.org/10.1016/j.gecco.2016.07.005.

Rogers, K., Saintilan, N., Cahoon, D., 2005. Surface elevation dynamics in a regenerating mangrove forest at Homebush Bay, Australia. Wetl. Ecol. Manag. 13 (5), 587–598. https://doi.org/10.1007/s11273-004-0003-3.

Saintilan, N., Wilson, N.C., Rogers, K., Rajkaran, A., Krauss, K.W., 2014. Mangrove expansion and salt marsh decline at mangrove poleward limits. Glob. Chang. Biol. 20 (1), 147–157. https://doi.org/10.1111/gcb.12341.

Sapkota, Y., White, J.R., 2019. Marsh edge erosion and associated carbon dynamics in coastal Louisiana: a proxy for future wetland-dominated coastlines world-wide. Estuar. Coast. Shelf Sci. 226, 106289. https://doi.org/10.1016/j.ecss.2019.106289.

Schmidt, M.W.I., Torn, M.S., Abiven, S., Dittmar, T., Guggenberger, G., Janssens, I.A., Kleber, M., Kögel-Knabner, I., Lehmann, J., Manning, D.A.C., Nannipieri, P., Rasse, D.P., Weiner, S., Trumbore, S.E., 2011. Persistence of soil organic matter as an ecosystem property. Nature 478 (7367), 49–56. https://doi.org/10.1038/nature10386.

Simpson, L.T., Cherry, J.A., Smith, R.S., Feller, I.C., 2021. Mangrove encroachment alters decomposition rate in saltmarsh through changes in litter quality. Ecosystems 24 (4), 840–854. https://doi.org/10.1007/s10021-020-00554-z.

Six, J., Frey, S.D., Thiet, R.K., Batten, K.M., 2006. Bacterial and fungal contributions to carbon sequestration in agroecosystems. Soil Sci. Soc. Am. J. 70 (2), 555–569. https://doi.org/10.2136/sssaj2004.0347.

Sokol, N.W., Sanderman, J., Bradford, M.A., 2019. Pathways of mineral-associated soil organic matter formation: integrating the role of plant carbon source, chemistry, and point of entry. Glob. Chang. Biol. 25 (1), 12–24. https://doi.org/10.1111/gcb.14482.

Sparks, D.L., Page, A.L., Helmke, P.A., Loeppert, R.H., Soltanpour, P.N., Tabatabai, M.A., Johnston, C.T., Sumner, M.E., 1996. Methods of Soil Analysis: Part 3 Chemical Methods, 1st ed. 5. Wiley. https://doi.org/10.2136/sssabookser5.3.

Steinmuller, H.E., Breithaupt, J.L., Engelbert, K.M., Assavapanuvat, P., Bianchi, T.S., 2022. Coastal wetland soil carbon storage at mangrove range limits in Apalachicola Bay, FL: observations and expectations. Front. Forest Glob. Change 5, 852910. https://doi.org/10.3389/ffgc.2022.852910.

Sterner, R.W., Elser, J.J., 2002. Ecological stoichiometry: the biology of elements from molecules to the biosphere. Princeton University Press. http://www.jstor.org/stable/j.ctt1jktrp3.

Tang, Y., Horikoshi, M., Li, W., 2016. Ggfortify: unified Interface to visualize statistical results of popular R packages. R Journal 8 (2), 474. https://doi.org/10.32614/RJ-2016-060.

Turner, R.E., Howes, B.L., Teal, J.M., Milan, C.S., Swenson, E.M., Goehringer-Toner, D. D., 2009. Salt marshes and eutrophication: an unsustainable outcome. Limnol. Oceanogr. 54 (5), 1634–1642. https://doi.org/10.4319/lo.2009.54.5.1634.

Upreti, K. (2019). Evaluating Seasonal Nutrient Fluxes in Emerging and Eroding Wetlands of the Louisiana Delta Plain [Doctor of Philosophy, Louisiana State University and Agricultural and Mechanical College]. Doi:10.31390/gradschool_dissertations.4814.

USDA NRCS, 2011. Soil survey laboratory information manual (Soil Survey Investigations Report No.45). USDA NRCS.

USEPA. (1993). Methods for determination of inorganic substances in environmental samples. EPA/600/R-93/100.

Valiela, I., Cole, M.L., 2002. Comparative evidence that salt marshes and mangroves may protect seagrass meadows from land-derived nitrogen loads. Ecosystems 5 (1), 92–102. https://doi.org/10.1007/s10021-001-0058-4.

Vaughn, D.R., Bianchi, T.S., Shields, M.R., Kenney, W.F., Osborne, T.Z., 2020. Increased organic carbon burial in Northern Florida mangrove-salt marsh transition zones. Glob. Biogeochem. Cycles 34 (5), e2019GB006334. https://doi.org/10.1029/2019GB006334.

Vaughn, D.R., Bianchi, T.S., Shields, M.R., Kenney, W.F., Osborne, T.Z., 2021. Blue carbon soil stock development and estimates within northern Florida wetlands. Front. Earth Sci. 9, 552721. https://doi.org/10.3389/feart.2021.552721.

Vervaeke, W.C., Feller, I.C., Jones, S.F., 2025. Ongoing range shift of mangrove foundation species: *Avicennia germinans* and *Rhizophora mangle* in Georgia, United States. Estuar. Coasts 48 (3), 78. https://doi.org/10.1007/s12237-025-01501-8.

Von Lützow, M., Kögel-Knabner, I., Ekschmitt, K., Flessa, H., Guggenberger, G., Matzner, E., Marschner, B., 2007. SOM fractionation methods: relevance to functional pools and to stabilization mechanisms. Soil Biol. Biochem. 39 (9), 2183–2207. https://doi.org/10.1016/j.soilbio.2007.03.007.

Wang, X., Chen, R.F., Cable, J.E., Cherrier, J., 2014. Leaching and microbial degradation of dissolved organic matter from salt marsh plants and seagrasses. Aquat. Sci. 76 (4), 595–609. https://doi.org/10.1007/s00027-014-0357-4.

Weaver, C.A., Armitage, A.R., 2020. Above- and belowground responses to nutrient enrichment within a marsh-mangrove ecotone. Estuar. Coast. Shelf Sci. 243, 106884. https://doi.org/10.1016/j.ecss.2020.106884.

Wickham, H., 2016. Ggplot2. Springer International Publishing. https://doi.org/10.1007/978-3-319-24277-4.

Wickham, H., Averick, M., Bryan, J., Chang, W., McGowan, L.D., François, R., Grolemund, G., Hayes, A., Henry, L., Hester, J., 2019. Welcome to the tidyverse. J. Open Source Softw 4 (43), 1686. https://doi.org/10.21105/joss.01686.

Wigand, C., Roman, C.T., Davey, E., Stolt, M., Johnson, R., Hanson, A., Watson, E.B., Moran, S.B., Cahoon, D.R., Lynch, J.C., Rafferty, P., 2014. Below the disappearing marshes of an urban estuary: historic nitrogen trends and soil structure. Ecol. Appl. 24 (4), 633–649. https://doi.org/10.1890/13-0594.1.

Wood, N., Hine, A.C., 2007. Spatial trends in marsh sediment deposition within a Microtidal Creek System, Waccasassa Bay, Florida. J. Coast. Res. 234, 823–833. https://doi.org/10.2112/04-0243.1.

Worthington, T.A., Zu Ermgassen, P.S.E., Friess, D.A., Krauss, K.W., Lovelock, C.E., Thorley, J., Tingey, R., Woodroffe, C.D., Bunting, P., Cormier, N., Lagomasino, D., Lucas, R., Murray, N.J., Sutherland, W.J., Spalding, M., 2020. A global biophysical typology of mangroves and its relevance for ecosystem structure and deforestation. Sci. Rep. 10 (1), 14652. https://doi.org/10.1038/s41598-020-71194-5.

Zhang, J., Gan, S., Yang, P., Zhou, J., Huang, X., Chen, H., He, H., Saintilan, N., Sanders, C.J., Wang, F., 2024. A global assessment of mangrove soil organic carbon sources and implications for blue carbon credit. Nat. Commun. 15 (1), 8994–8997. https://doi.org/10.1038/s41467-024-53413-z.

Zhang, X., Liu, S., Wu, Y., Luo, H., Ren, Y., Liang, J., Huang, X., Macreadie, P.I., 2025. Nutrient loading accelerates breakdown of refractory dissolved organic carbon in seagrass ecosystem waters. Water Res. 273, 123017. https://doi.org/10.1016/j.watres.2024.123017.